# COMPRESSIVE BEHAVIOR OF TRABECULAR BONE IN THE PROXIMAL

# TIBIA USING A CELLULAR SOLID MODEL

A Dissertation

by

DANU PROMMIN

Submitted to the Office of Graduate Studies of
Texas A&M University
in partial fulfillment of the requirements for the degree of

DOCTOR OF PHILOSOPHY

August 2004

Major Subject: Biomedical Engineering

# COMPRESSIVE BEHAVIOR OF TRABECULAR BONE IN THE PROXIMAL

# TIBIA USING A CELLULAR SOLID MODEL

A Dissertation

by

DANU PROMMIN

Submitted to Texas A&M University
in partial fulfillment of the requirements
for the degree of

DOCTOR OF PHILOSOPHY

Approved as to style and content by:

| | |
|---|---|
| _____ | _____ |
| William A. Hyman | Hsin-i Wu |
| (Chair of Committee) | (Member) |
| | |
| _____ | _____ |
| John C. Criscione | Donald A. Hulse |
| (Member) | (Member) |
| | |
| _____ | |
| William A. Hyman | |
| (Head of Department) | |

August 2004

Major Subject: Biomedical Engineering

**ABSTRACT**

Compressive Behavior of Trabecular Bone in the Proximal Tibia Using a Cellular Solid

Model. (August 2004)

Danu Prommin, B.Eng., King Mongkut's Institute of Technology, Thonburi;

M.S., Texas A&M University

Chair of Advisory Committee: Dr. William A. Hyman

In this study, trabecular architecture is considered as a cellular solid structure, including both intact and damaged bone models. "Intact" bone models were constructed based on ideal versions of 25, 60 and 80-year-old specimens with varying trabecular lengths and orientations to 5%, and 10% covariance of variation (COV). The models were also flipped between longer transverse and longer longitudinal trabeculae. With increasing COV of lengths and orientations of trabecular bone, the apparent modulus is linearly decreased, especially in the longer transverse trabeculae lengths. "Damaged" bone models were built from the 25 year old model at 5% COV of longer transverse trabeculae, and with removing trabeculae of 5% and 10% of trabecular volume in transverse and longitudinal directions, respectively, as well as in combination to total 10% and 15%. With increasing percent of trabeculae missing, the apparent modulus decreased, especially dramatically when removal was only in the transverse direction. The trabecular bone models were also connected to a cortical shell and it was found that the apparent modulus of an entire slice was increased in comparison to the modulus of

trabecular bone alone. We concluded that the architecture of trabecular bone, especially both lengths and percent of trabecular missing in the longitudinal direction, significantly influences mechanical properties.

# ACKNOWLEDGMENTS

# TABLE OF CONTENTS

**LIST OF FIGURES**

FIGURE                                                                                                    Page

# LIST OF TABLES

**CHAPTER I**

**INTRODUCTION**

Total knee replacement is a common surgery in the United States. According to the American Academic of Orthopaedic Surgeons (1), total knee replacements were performed on 245,000 patients in 1996, and revision surgeries were about eight percent of all knee replacement surgeries, each year in the U.S. It is predicted that total knee replacements will increase 85 percent from the 245,000 in 1996 to 454,000 by 2030 (17).

During primary total knee replacement the proximal aspect of the tibia and the distal aspect of the femur are removed with an oscillating saw and associated fixtures. The knee joint is resurfaced with metal components and a plastic insert made of ultra high molecular weight polyethylene is placed in between the metal components, attached to the tibial metal component. The metal components are either cemented into place using polymethylmethacrylate (bone cement) or press fit and allowed to adhere to the bone over time with a porous metal in contact with the bone. Screws may also be used. Many patients who need revision knee surgery require careful preoperative planning and a thorough knowledge of knee anatomy, biomechanics, and orthopedic implant characteristics because revision total knee surgery replacing a previously installed implant is frequently extremely complex. The surgeon often encounters destroyed bone and/or bone that has been compromised secondary to infection, polyethylene wear debris, or mechanical loading and local bone overload. The majority of failures are

_____
This dissertation follows the style and format of *Journal of Orthopaedic Research*.

secondary to loosening of the tibial implant component. It is not uncommon in revision surgery to find the bone stock of the tibia or the femur to be severely compromised. The surgeon must then restore the joint as best as possible to allow normal joint function and patient well-being. Orthopedic surgeons performing revision surgery can restore the joint with special implants, bone grafts (allograft or autograft), or bone cement. The surgeon's choice for reconstruction depends on experience, patient specifics, and the current orthopedic literature.

Sufficient strength of the cut tibial bone, especially trabecular bone, is crucial for adequate mechanical support and fixation, since the tibial tray component is placed directly on the underlying bone. Understanding the compressive behavior of both intact trabecular bone, and the cut tibial bone when loaded by the implant, are therefore very important. This is particularly true during revision surgery or in patients with compromised bone properties. The trabecular bone architecture depends on age, sex, diseases like osteoporosis, chemical activities such as drug abuse, and mechanical activities like space flight (4). These play an important role in the mechanical properties of bone. Many researchers have tried to model trabecular bone and better understand its mechanical behavior. The benefits are not only to predict appropriate bone cut level used to support a total knee prostheses, but also to predict the degree of osteoporosis or other degenerative conditions that need to be addressed during surgery.

The objective of this paper is to better understand the mechanical behavior of bone when trabeculae lengths and orientations are changed as well as when the percent of bone volume is decreased because of missing trabeculae, or when trabeculae breakage

occurs without measurable loss in bone volume. Here bone volume means the volume of the solid material rather that the overall volume defined by the bone contour. An additional objective is to understand how the direction of trabeculae lengths, and percent of missing trabeculae, influences the overall mechanical properties. This understanding may improve diagnoses associated with bone losses. Moreover, the trabecular simulation model was used to construct a whole slice model and, when connected to a cortical shell, to predict overall bone modulus. The overall bone model will allow better understanding of load transmission as well as normal and pathologic biomechanics. Finally, this study should assist in the development of future artificial knee joints.

# CHAPTER II

# BONE MECHANICS

## 2.1 BONE

A long bone is composed of diaphysis, metaphysis and epiphysis (Fig. 2.1a). The diaphysis consists of cortical bone, but the metaphysis and the epiphysis contain trabecular bone connected to a cortical shell. Moreover, the metaphysis and the epiphysis are wider than the diaphysis. Cortical bone is denser than trabecular bone as shown in Fig. 2.1b. In the overall adult human skeleton, the skeletal mass is 80% cortical bone and 20% trabecular bone (4). However, the distribution of cortical and trabecular bone are different among individual bones, and along the length of any one bone.

a.)            b.)
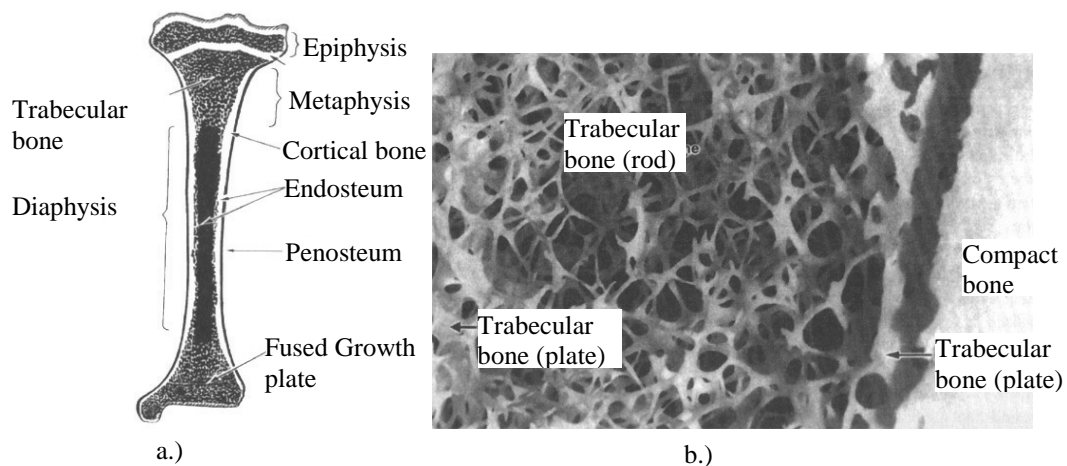
Fig. 2.1. a.) Diagram of a tibia bone b.) Trabecular bone architecture magnified from a tibia bone (10).

2.1.1 Mechanical Properties of Trabecular Bone

As shown in Table 2.1, most research papers on bone mechanical properties used apparent density, or the ratio of bone volume to total volume, BV/TV, for prediction of overall mechanical properties of a trabecular bone model without considering detailed structure. The resulting equations were derived from mechanical experiments using regression analysis. Carter et al (3) showed that the apparent elastic modulus of trabecular bone is proportional to the third power of apparent density, but the compressive strength is related to the square of apparent density of trabecular bone. They also found that the strain rate has no effect on compressive properties except for strain rates higher than 10.0 per second. Gibson (5) showed, from analyzed experiment data, that the power law of apparent density is two for modulus of elasticity if the density is lower than 350 kg.m$^{-3}$, while the power law exponent at higher densities is three. He suggested from his results that a cellular model changes from rod-like to plate-like at a density of about 350 kg.m$^{-3}$. However, the power law for overall apparent densities was found to be two for yield strength. Rice et al (19) analyzed statistical data from many previous papers and concluded that both the modulus of elasticity and the yield strength of trabecular bone are related to the square of apparent density of trabecular bone. Yeni et al (27) presented from their experimental data that bone volume fraction could be used to determine mechanical properties. The volume fraction is proportional to the relative density assuming that apparent bone mass is equal to trabeculae bone mass. Their results showed that the relationship between volume fraction and ultimate strength is linear, not power law, for either glued or platen loading surfaces. Moreover, they did not use the volume

Table 2.1. Summary of experimental results on trabecular bone from previous research

| Source | Type of bone | Size of specimen | Mechanical relationships |
|---|---|---|---|
| Carter & Hayes (3) | Bovine, Human | $\phi20.6\times5$mm Cylinder | $E = 3790\dot{\varepsilon}^{0.06}\rho^3$, $\sigma_c = 68\dot{\varepsilon}^{0.06}\rho^2$, $\rho_s = 1.8$g/cm$^3$, $\sigma_s = 221$MN/m$^2$ $E_s = 2.21\times10^4$ MN/m$^2$ where $E$, $\sigma_c$ (MN/m$^2$), $\rho$ (g/cm$^3$) |
| Gibson (5) | Bovine, Human: | Pooled data then use statistical analysis | Relative density > 0.2 (at $\rho = 350$ kg/m$^3$): $E \propto \rho^3$, $\sigma_c \propto \rho^3$ Relative density < 0.2: $E$ and $\sigma_c \propto \rho^2$ where $E$, $\sigma_c$ (MN/m$^2$), $\rho_s = 1800$ kg/m$^3$ |
| Hvid (9) | Human tibia | $\phi7.5\times7.5$mm Cylinder | Destructive compression tests $E = 1371\rho^{1.33}$, $\sigma_u = 25.30\rho^{1.494}$ Non-destructive compression tests $E = 2132\rho^{1.46}$ $\sigma = 6.16\rho^{1.13}$ where $E$, $\sigma_u$ (MPa), $\rho$ (g/cm$^3$) |
| Keaveny (12) | Bovine tibia | $\phi8\times40$mm Cylinder | $\sigma_{yt} = 5.630\times10^{-3}E+C_1$, $\sigma_{yc} = 9.580\times10^{-3}E+C_2$ where $C_1$, $C_2$ = Constant, $\rho = 1.62$QCT-1.36, $\sigma_{yt} = 76.9$QCT-77.8, $\sigma_{yc} = 169$QCT-184 where $E$, $\sigma_{yt}$, $\sigma_{yc}$ (MPa), $\rho$, QCT (g/cm$^3$) |
| Keyak (13) | Human tibia | $15\times15\times15$ mm | $E = 33900\rho_a^{2.20}$ $\sigma = 137\rho_a^{1.88}$, $\rho_a = 0.551\rho-0.00478$, where $E$, $\sigma$ (MPa), $\rho$, $\rho_a$ (g/cm$^3$) |
| Majumdar (15) | Human Calcaneus, Femur, and Vertebral | $12\times12\times12$ mm | $E$ (Mpa) $\propto$ BMD(mg/cm$^3$) |
| Rice (19) | Bovine, Human | Pooled data then use statistical analysis | Bovine: $E= 0.006+3.24\rho^2$ for tension $E= 0.006+2.49\rho^2$ for compression $\sigma = 2.45+63.05\rho^2$ Human: $E = 0.006+1.65\rho^2$ for tension $E = 0.006+0.90\rho^2$ for compression $\sigma = 2.45+32.66\rho^2$ where $E$(GPa), $\sigma$(MPa), $\rho$ (g/cm$^3$) |
| Rφhl (20) | Human tibia | 20mm thickness | $E_c = 222r_0^{11.4}$, $E_t = 228r_0^{11.1}$, $\sigma_{uc} = 1.2r_0^{12.7}$, $\sigma_{ut} = 1.6r_0^{10.7}$ where $E_c$, $E_t$, $\sigma_{uc}$, $\sigma_{ut}$ (MPa), $r_0$ (unitless) |
| Wolf (25) | Human Femur | Using QCT | $E$ (Mpa) $\propto$ BMD(mg/cm$^3$) raised to a power |
| Yeni (27) | Human vertebral | $\phi8\times9.5$mm Cylinder | Platens loading: $\sigma_u = 0.0103E_{exp}+0.0148$, $\sigma_u = 30.9$BV/TV-1.58, $\sigma_u = 0.0143E_{FEM}-0.488$ Glued loading: $\sigma_u = 0.0044E_{exp}+0.929$, $\sigma_u = 53.0$BV/TV-4.59, $\sigma_u = 0.0145E_{FEM}-0.354$ where $\sigma_u$, $E_{exp}$, $E_{FEM}$ (MPa), BV/TV (m$^3$/m$^3$) |

Where

$\sigma_c$ , $\sigma_t$ , $\sigma_u$ apparent compressive, tensile, and ultimate strength, respectively
$\sigma_{yc}$ , $\sigma_{yt}$ apparent yield strength for compression and tension, respectively
$E_s$ Trabeculae modulus (solid material modulus or compact bone modulus)
$E$ Apparent trabecular bone modulus
BV , TV Bone volume and total volume, respectively
BV/TV Volume fraction
$\rho$ , $\rho_a$ , $\rho_s$ Apparent, ash, and trabeculae density, respectively
$L_t$, $L_l$ Trabeculae length in transverse and longitudinal direction, respectively
$d_t$, $d_l$ Trabeculae diameter in transverse and longitudinal direction, respectively
$r_0$ relative attenuation coefficient
$\varepsilon$ strain and $\dot{\varepsilon}$ strain rate
QCT density measured by CT (g/ml of $K_2PO_4$)
$\nu$ Poisson ratio

fraction to predict modulus of elasticity. They used linear regression analysis to determine the relationship between experimental modulus and ultimate strength.

In addition to the relationship between mechanical properties and apparent density, many researchers have tried to find different relationships using bone mineral density (BMD) obtained from X-ray quantitative computed tomography, QCT, or using ash density i.e. matrix density. For example, Røhl and his colleague (20) use the relative linear attenuation coefficient $r_0$, which is converted from CT value, to find statistically the relationship with mechanical parameters such as coefficient of elasticity, work to failure, and strength. Røhl et al found that both coefficient of elasticity and strength, and work of failure are proportional to $r_0$ raised to a power of about 10.7-12.2, and 9.0-14.4, respectively, but they found no relationship with ultimate strain. Hvid et al (9) used the CT value, apparent density and ash density to find the relationship with mechanical properties. They determined the power law value of the CT value, which is related to modulus of elasticity and strength, to be about 6.96-9.15, which is similar to Røhl's results. They also found that the CT value could predict the mechanical properties in a linear relationship with a high correlation coefficient. Moreover, their results showed that apparent density is linearly related to ash density and they preferred the power law regression model to predict the mechanical relationship by using apparent density more than linear regression even though the correlation coefficients of both linear and power law regression are not really different. Keaveny et al (12) also found that the CT value was related to the trabecular strength with a linear relationship instead of the power law relationship of Hvid and Røhl. They also found that the apparent modulus of trabecular

bone was linearly related to the trabecular strength. In addition to Hvid, Røhl and Keaveny's paper, Wolf et al (25) graphically showed that the BMD is related to the modulus of elasticity but Wolf et al did not formulate a final model. However, from their graph, it looks like a quadratic equation, which can be fit by power law regression. In another example of the use of ash density to predict mechanical properties, Keyak et al (13) used CT to calibrate with density and ash density, and found that both modulus of elasticity and strength are proportional to ash density raised to a power of about 2.20 and 1.88, respectively. Majumdar (15) also use BMD to predict the mechanical relationship. However, the relationship of mean elastic modulus and BMD showed two different slopes for the proximal femur and vertebrae.

Finally, from Table 2.1 all equations were converted to have the same units of apparent modulus ($N/m^2$), apparent strength ($N/m^2$), and density ($m^3$) as shown in Table 2.2. Thereafter, referring to Table 2.2, the relationships between the apparent modulus and BV/TV were plotted in Fig. 2.2, as well as the relationships between the apparent strength and BV/TV in Fig. 2.3. Trabeculae density was assumed at $1.8 \times 10^3$ kg/$m^3$ for all relationship. From these graphs, it appears that apparent density cannot accurately predict the mechanical properties of trabecular bone. This can be attributed at least in part to the lack of correlation between apparent density and trabecular architecture as will be addressed further below.

2.1.2 Mechanical Properties in Different Trabecular Architectures

Trabecular bone structure is composed of a network of tiny rods and plates of trabeculae (Fig. 2.1b). Therefore, treating the bone in accordance with the theory of

Table 2.2. Summary of unit conversion from Table 2.1 where unit of all E, $\sigma$ is N/m$^2$ and unit of all $\rho$ is kg/m$^3$

| Source | Mechanical relationships |
|---|---|
| Carter & Hayes (3) | $E = 2.875\rho^3$, $\sigma_c = 5.1583 \times 10^2 \rho^2$ at strain rate 0.01 (1/s), $\rho_s = 1.800 \times 10^3$ kg/m$^3$, $\sigma_s = 2.21 \times 10^8$ N/m$^2$, and $E_s = 2.21 \times 10^{10}$ N/m$^2$ |
| Gibson (5) | Relative density > 0.2 ($\rho = 3.500 \times 10^2$ kg/m$^3$): $E \propto \rho^3$, $\sigma_c \propto \rho^3$ <br> Relative density < 0.2: E and $\sigma_c \propto \rho^2$, $\rho_s = 1.800 \times 10^3$ kg/m$^3$ |
| Hvid (9) | Destructive compression tests (1): $E = 1.403 \times 10^5 \rho^{1.330}$, $\sigma_u = 8.339 \times 10^2 \rho^{1.494}$ <br> Non-destructive compression tests (2): $E = 8.888 \times 10^4 \rho^{1.460}$ $\sigma = 2.509 \times 10^3 \rho^{1.130}$ |
| Keaveny (12) | $\sigma_{yt} = 5.630 \times 10^{-3}E + C_1$(1), $\sigma_{yc} = 9.580 \times 10^{-3}E + C_2$ (2) where assuming $C_1, C_2 = -0.010 \times 10^6$ N/m$^2$, $\rho = 1.620$QCT$-1.360 \times 10^3$, $\sigma_{yt} = 7.690 \times 10^4$QCT$-7.780 \times 10^7$ (3), $\sigma_{yc} = 1.690 \times 10^5$QCT$-1.840 \times 10^8$ (4) |
| Keyak (13) | $E = 8.515 \times 10^3 \rho_a^{2.20}$, $\sigma = 3.138 \times 10^2 \rho_a^{1.88}$, $\rho = 0.551 \rho_a - 4.780$ |
| Majumdar (15) | $E \propto$ BMD |
| Rice (19) | Bovine: $E = 6.000 \times 10^6 + 3.240 \times 10^3 \rho^2$ for tension (1), <br> $E = 6.000 \times 10^6 + 2.490 \times 10^3 \rho^2$ for compression (2), $\sigma = 2.450 \times 10^6 + 6.305 \times 10^2 \rho^2$ (3) <br> Human: $E = 6.000 \times 10^6 + 1.650 \times 10^3 \rho^2$ for tension (4), <br> $E = 6.000 \times 10^6 + 0.900 \times 10^3 \rho^2$ for compression (5), $\sigma = 2.450 \times 10^6 + 3.266 \times 10^2 \rho^2$ (6) |
| Røhl (20) | $E_c = 2.220 \times 10^8 r_0^{11.4}$, $E_t = 2.280 \times 10^8 r_0^{11.1}$, $\sigma_{uc} = 1.200 \times 10^6 r_0^{12.7}$, $\sigma_{ut} = 1.600 \times 10^6 r_0^{10.7}$ where $r_0$ is unit less |
| Wolf (25) | $E \propto$ BMD raised to a power |
| Yeni (27) | Platens loading: <br> $\sigma_u = 1.030 \times 10^{-2}E_{exp} + 1.480 \times 10^4$ (1), $\sigma_u = 3.090 \times 10^7$BV/TV$-1.580 \times 10^6$ (2), <br> $\sigma_u = 1.430 \times 10^{-2}E_{FEM} - 4.880 \times 10^5$ (3) <br> Glued loading: <br> $\sigma_u = 4.400 \times 10^{-3}E_{exp} + 9.290 \times 10^5$ (4), $\sigma_u = 5.300 \times 10^7$BV/TV$-4.590 \times 10^6$ (5), <br> $\sigma_u = 1.450 \times 10^{-2}E_{FEM} - 3.540 \times 10^5$ (6) |
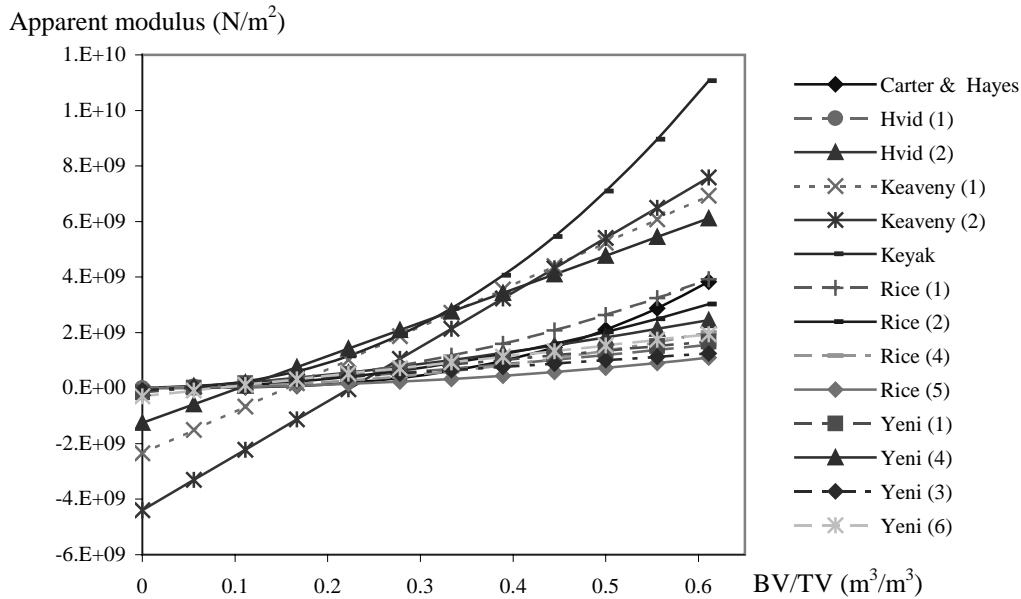


Fig. 2.2. The relationship between apparent modulus and BV/TV from previous research referring to Table 2.2.

Apparent strength (N/m$^2$)
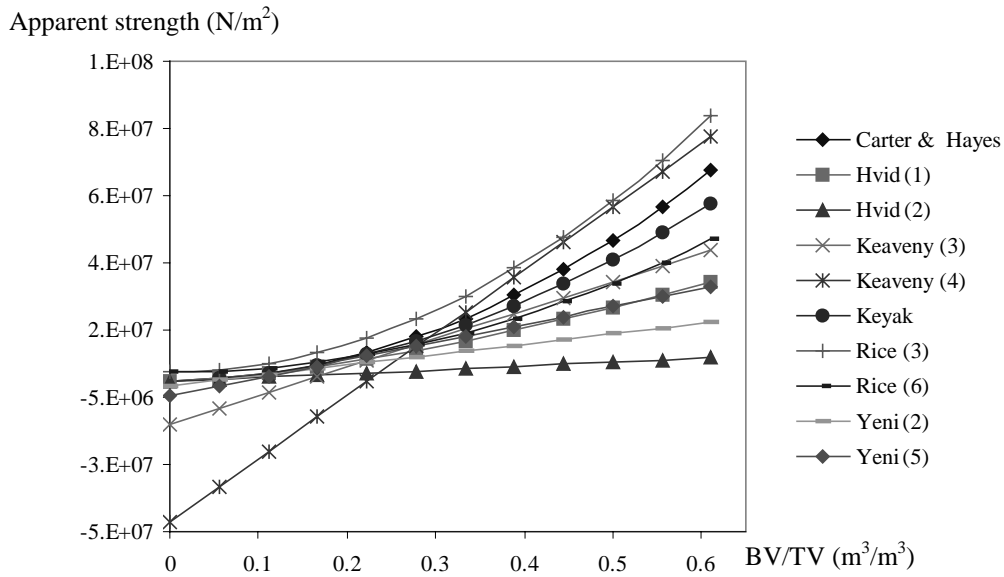


Fig. 2.3. The relationship between apparent strength and BV/TV from previous research referring to Table 2.2.
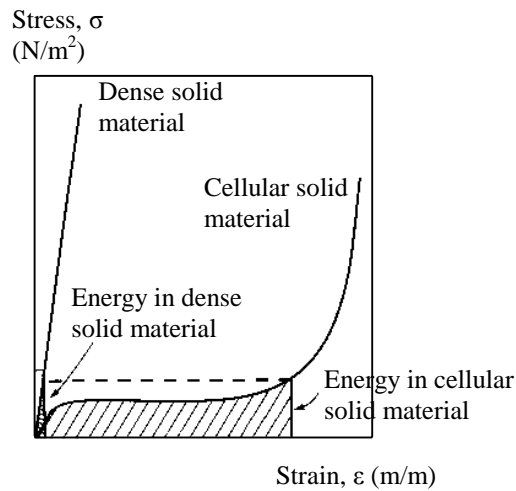


Fig. 2.4. Comparison of compressive stress-strain relationship between a cellular solid (foam for this case) and a fully dense solid (6).

cellular solids offers a promising approach. In the theory of cellular solid materials, the

ratio of bulk density to the material density plays an important role in the overall stress-

strain relationship and in energy absorption (6) under ideal and consistent geometries. The yield compressive stress of a cellular solid is normally lower than its solid constituent alone, but the energy absorption of a cellular solid is higher because it typically allows extended strain at the yield stress before densification occurs (Fig. 2.4). Røhl et al (20) studied the tensile and compressive properties of trabecular bone and their results showed that strain is extended to 5 % after the initial yield strength. Their study involved destructive testing, and this result is similar to the properties of certain cellular materials (Fig. 2.4). Gibson et al (6) showed that the ratio of the bulk modulus to the matrix modulus, i.e. relative modulus, is proportional to the squared ratio of the bulk density to the matrix density, i.e. relative density, for the cubic open cell model and proportional to the cubic ratio of relative density for cubic closed cell model. However, as suggested by Keaveny et al (12), the mechanical properties actually depend in a more detailed way on the magnitude of the porosity i.e. apparent density, trabecular architecture, and material properties of the tissue in the individual trabeculae. Therefore, apparent density or matrix density may not be enough to predict the mechanical properties.
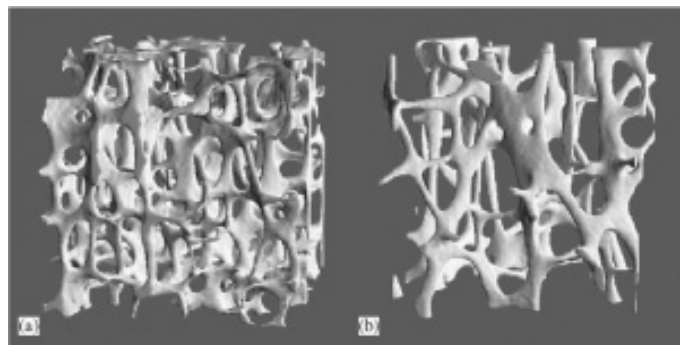


Fig. 2.5. Sample of a) healthy bone and b) osteoporosis bone (7).

Hogan et al (8) showed that rat ovariectomized groups (OVX) had lower ultimate strength, modulus of elasticity, and energy at maximum force compared with sham groups. Like osteoporosis (4,7) and aged bone (4,14) (Fig. 2.5), OVX will change not only apparent density but architecture of trabecular bone and material properties of individual trabeculae as well. Cowin (4) reported that both elastic modulus of vertebral trabecular tissue and cortical tissue decease when people get older than 40 years old. In addition to age and bone disease, like osteoporosis, bone loss depends on sex, chemical activities such as drug abuse, and mechanical activities like space flight.

2.1.3 Trabecular Bone Model

As shown in Table 2.3, there are some previous studies that simulated the architecture of trabecular bone to show that trabecular structure plays an important role in mechanical properties. Jensen, Kim and Yeh's models (11,14,26) varied the trabecular space and thickness related to age. Jensen et al (11) used relative lattice disorder to model from a simple rectangular lattice to a non-uniform cubic lattice. When they increased the value of the relative lattice disorder, the mechanical properties decreased. In addition, increase of trabecular space and decrease of trabecular diameter corresponding with age had effects on the mechanical properties similar to experiment data. They concluded that the measurements of apparent density should be as important as the measurements of trabecular bone architecture. Yeh et al (26) followed Jensen et al's ideas and found that when they decreased volume fraction, i.e. relative density, in the model by reducing the thickness of trabeculae, the mechanical properties linearly decreased. They also used coefficient of variation, COV, to distribute trabecular thickness and showed that an

Table 2.3. Summary of trabecular bone model from previous research

| Source | Architecture of Trabeculae | | | | | Mechanical properties of Trabeculae | Generating trabecular bone models |
|---|---|---|---|---|---|---|---|
| Jensen (11) | Ideal rectangular lattice in three dimension with round trabeculae: | | | | | $E = 11.4$ GPa $\nu = 0.3$ | Perturbed lengths by relative lattice disorder constants, $\alpha$ of 0.3, 0.6, 1.0. $L_{model} = L_{avg} + \alpha L_{avg} X$ where X is randomly drawn from Uniform distribution on interval from -½ to ½. Fixed trabeculae diameters |

| Age years | Trabeculae dimension | | | |
|---|---|---|---|---|
| | $L_t$ (µm) | $L_l$ (µm) | $d_t$ (µm) | $d_l$ (µm) |
| 40 | 720 | 770 | 150 | 210 |
| 60 | 870 | 1110 | 125 | 210 |
| 80 | 990 | 1450 | 95 | 210 |

| Source | Architecture of Trabeculae | Mechanical properties of Trabeculae | Generating trabecular bone models |
|---|---|---|---|
| Kim (14) | Ideal hexagonal columnar structure with 2 models of uniform (round) and tapered trabeculae. Length and diameter of trabeculae depend on age and sex-related from report's Mosekilde (1998,1999) | $E = 12$ Gpa $\sigma_y = 193$ MPa | Perfectly columnar structure. No perturbed length, diameter and orientation. |
| Silva (22) | Ideal squared lattice of 1 by 1 mm in two dimension with round trabeculae | $E = 1$ Mpa, $\sigma_y = 0.01$ MPa $\nu = 0.3$ | "Intact" model: Perturbed Voronoi diagram using Fortran computer software. "Aged" model: Randomly remove trabeculae from "Intact" model with 5% 10% and 15% reduction of bone volume either from longitudinal or from transversal direction. "Treated" model: Increasing thickness from "Aged" model. |
| Yeh (26) | Ideal rectangular lattice in three dimension with round trabeculae: | $E = 13$ GPa $\nu = 0.3$ | Perturbed lengths by a relative lattice disorder constant, $\alpha$ of 0.6 (one of Jensen's model). Varied diameters by using 25%, 40%, and 55%COV of average diameter. |

| Age years | Trabeculae dimension | | | |
|---|---|---|---|---|
| | $L_t$ (µm) | $L_l$ (µm) | $d_t$ (µm) | $d_l$ (µm) |
| 25 | 624 | 631 | 164 | 215 |
| 50 | 791 | 973 | 139 | 215 |
| 80 | 992 | 1384 | 109 | 215 |

increase in COV decreased the overall mechanical properties. Silva et al (22) used a Voronoi diagram to model from 2D square meshes to perturbed 2D meshes. Their results showed that reductions in the number of trabeculae decreased the mechanical properties more than uniformly decreasing the thickness of trabeculae to the same loss of bone

volume. They also found that when they increased the trabeculae thickness but not the number of trabeculae in a reduced trabecular model, simulating the effect of some drug treatments, the mechanical properties increased but were still only 37% as strong as the intact trabeculae. Kim (14) constructed a hexagonal columnar trabecular model with uniform and tapered trabeculae, instead of a rectangular trabecular model. They showed that mechanical properties of trabecular bone decrease as result of changes of trabecular space and diameters associated with aging. In addition, the apparent modulus of the tapered trabeculae model was higher than of uniform trabeculae.

The results from the variation of trabecular architecture of intact models from previous research illustrate some effects on mechanical properties. However, bone loss caused by age, some diseases, or mechanical activities result in changes in bone formation with missing trabeculae instead of loss in quantity. Osteoporosis, for example, is a decrease in bone mass and a deterioration in bone microarchitecture, which lead to enhance fragility of the skeleton, and therefore to a higher risk of fracture (4). Therefore, ignoring the fact that bone loss is not only a loss in bone mass but also involves changes in trabecular architecture may result in a failure in fully understanding the mechanical properties of trabecular bone. Many researchers have also tried to find treatment for bone loss such as using drugs, or exercise in restoring the bone mass. They found that each drug treatments such as bisphosphonates and MDL 103,323 show different effects on the mechanical properties of trabecular bone. Bisphosphonates have been shown to increase bone mass and decrease fracture risk in postmenopausal osteoporotic women. However, bisphosphonates prevents the repair of microdamage by suppressing bone

remodeling (16). When microdamage accumulates there is a reduction in the mechanical properties. This situation reflects an increase in mass that does not translate into increased strength. Unlike the effects of bisphosphonates, MDL 103,323 did not restore the trabecular bone lost, but trabecular formation was slightly elevated as compared with sham (2). This could improve the mechanical properties of trabecular bone. In addition to bisphosphonates and MDL 103,323 effect, residronate reduces fracture risk by creating more uniform trabeculae, thus preventing buckling of the compressively loaded longitudinal trabeculae in particular (24). MDL 103,323 and residronate showed that improvement of architecture of trabecular bone by using drug treatment increases the mechanical properties. The results are constant with the mechanical results obtained here which show the effect of architecture on mechanical properties not only from changes in bone space and variation of bone space but also changes in trabeculae formation by removing trabeculae in both random and stress based models. In addition to study in trabecular model alone, this study also considered the trabeculae network connected to a cortical shell model to better understand the overall mechanical properties of bone.

## 2.2 MECHANICS OF THE KNEE

### 2.2.1 Knee Structure

The main bony parts of the knee are the femur, tibia, fibula, and patella. The femur is the large bone of the thigh; the tibia is the large bone of lower leg; the fibula is the small bone of the lower leg; and the patella (kneecap) is the fourth bone of the knee joint. The knee joint structure is primarily of the hinge type; the knee, therefore, mainly allows rotation approximately about a single axis. Important ligaments connect the
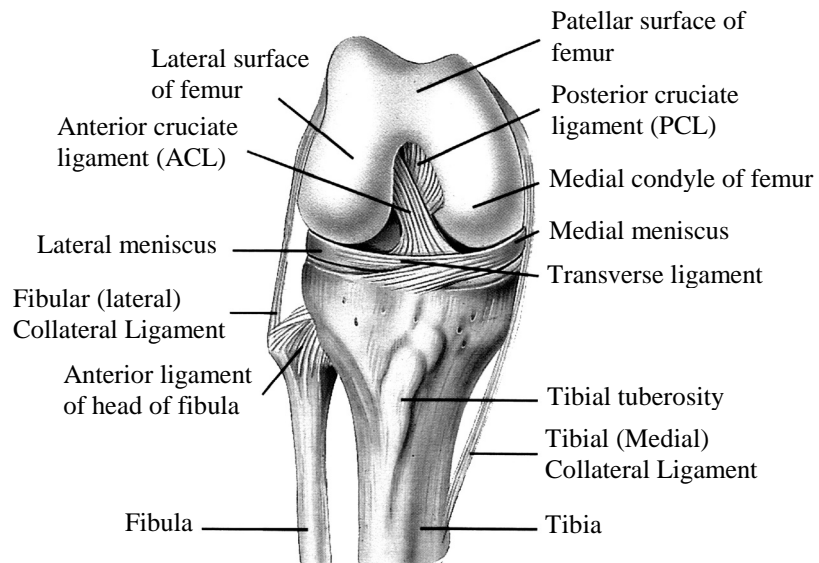
Fig. 2.6. Anterior of right flexed knee joint (23).
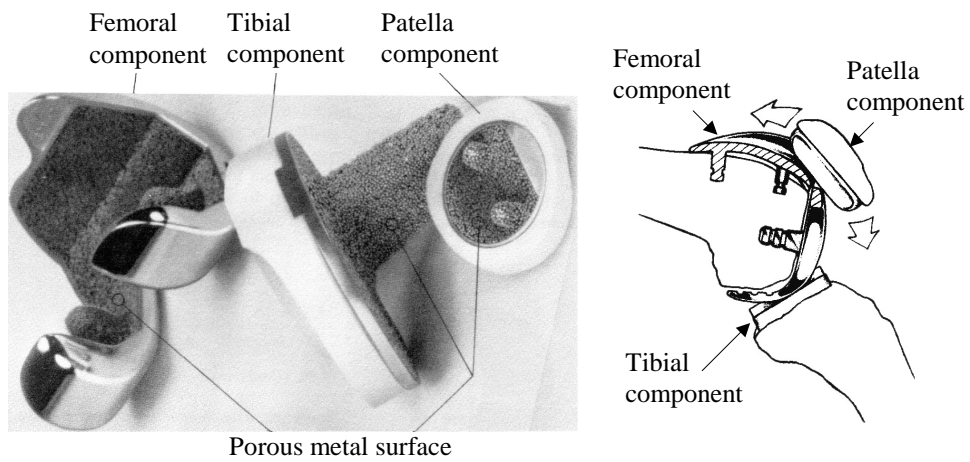


Fig. 2.7. Three parts of total knee replacement (18).

femur and tibia (Fig. 2.6). Two ligaments, the medial collateral ligament and the lateral collateral ligament, are found on either side of the knee joint. They restrain the movement of the knee joint in the side-to-side (lateral-medial) direction. The other ligaments, anterior cruciate ligament (ACL) and posterior cruciate ligament (PCL), act inside the knee joint to limit movement in the front to back (anterior-posterior) direction. The articular cartilage covers the ends of each bone, thus allowing the surfaces to roll and slide against one another without damage to either surface under normal conditions. Moreover, the space between distal femur and proximal tibia is filled with the medial and lateral meniscus to protect the articular cartilage from excessive force.

2.2.2 Total Knee Replacement

The main reason for total knee replacement surgery is degeneration of the knee joint articular cartilage, caused mostly from osteoarthritis, gouty arthritis, or abnormalities of knee joint function. One result of the resulting bone rubbing against bone in the absence of articular cartilage is pain. The typical total knee replacement is made up of three parts: the tibial component, the femoral component, and the patellar component (Fig. 2.7). The tibial component replaces the proximal tibia. It is usually made up of two parts, a metal tray (typically a cobalt-chrome or titanium alloy) that is attached to the bone and a plastic insert that provides the bearing surface. The plastic insert is typically made of ultra high molecular weight polyethylene (UHMWPE). The tibial tray may be of a stem or stem-less design. The femoral component, usually made of metal, replaces the two femoral condyles and the groove where the patella runs. The

patellar component (usually also UHMWPE) replaces the joint surface on the bottom of the patella where it rubs against the femur in the femoral groove.

The metal components of a total knee replacement can be cemented or uncemented. Screws may also be used. For the cemented prosthesis polymethyl-methacrylate (bone cement) is used to attach the metal to the bone, which is especially needed for the stem-less tibial tray. The uncemented prosthesis typically has a porous metal surface into which bone grows to attach the prosthesis to the bone. There are several manufacturers of total knee replacements with various models available. However, regardless of claims of competitive advantage, the basic configuration of each device is similar (18,21).

To prepare the bone for total knee replacement, the surgeon removes the ends of the bones by using an oscillating saw and appropriate jigs and fixtures that are intended to ensure good fit of the metal components to the bone. Thus, the surgeon removes several pieces of the distal femur, the proximal tibia, and the undersurface of the patella. Finally, the surgeon places each component to the remaining bone (Fig. 2.7).

The standard surgery involves removing about one centimeter of bone from the tibia, with the tibial component then resting on the remaining bone (21). In revision surgery, or surgery on more compromised bone, the surgeon often encounters destroyed bone, infection, joint stiffness, and thrombophlebitis. A majority of revisions are secondary to loosening of the tibial implant component, and loosening is often accompanied by loss of the underlying bone. Debris from the UHMWPE also plays an

important role in bone destruction, as phagocytes engulf the debris particles, accumulate, lyse, and release powerful, bone destroying enzymes (21).

2.3 RESEARCH PROSPECTIVE

In this research trabecular bone modeled as cellular solid structure is studied to understand more about overall mechanical properties and the behavior of the surgically cut tibia. The model provides considerable inside into the effects of trabecular geometry on bone mechanical properties. However, Hogan et al (8) showed that the mechanical properties of trabecular bone were different from a whole slice of bone, composed of trabecular bone and cortical bone. They showed that the apparent modulus and strength of trabecular bone were about 0.6 of both overall bone modulus and strength, respectively. Therefore, the mechanical properties of both trabecular bone (modeled as a cellular solid) and sliced bone as a composite material have been considered. In addition, of particular interest in this study is the influence on the mechanical properties of sliced bone of the stem of a tibial tray because of its effect on reducing the remaining proximal bone area. The metal tibial tray must be supported by the entire proximal end of the tibia that consists mostly of trabecular bone. Yet, it is the entire bone working as a unit that allows adequate support during ambulation. Therefore, the cross-sectional area of the stem will reduce the area of the bone, changing the overall mechanical properties.

In conclusion, this research is intended not only to study mechanical behavior of the trabecular bone alone, but also to understand the mechanical properties of a surgically modified whole bone. This work is part of the effort to allow precise decisions while planning a revision knee replacement, or primary surgery on otherwise

compromised bone. This may increase the success rate for either first total knee replacement or revision knee surgery.

In addition to the surgical relevance, a better understanding of the relationship between bone mechanical behavior and details of trabecular structure is relevant to understanding the effects of disease and other insults, and the effects of pharmaceutical, exercise and other treatments.

**CHAPTER III**

**MECHANICS OF MATERIALS**

3.1. BEAM

3.1.1. Axial Loading

Normal axial stress, $\sigma$, on a beam is the intensity of load, P, which is applied perpendicularly to the cross-sectional area, A, of that beam as shown in Fig. 3.1. There are two types of normal stress, tensile and compressive, depending on the direction of loading. When the load is axially pulled outward from the beam, the beam is stretched, thus defining tensile stress. Reversing the load direction causes compression of the beam, thus defining compressive stress. The following equation expresses the magnitude of normal axial stress.

$$\sigma = P/A \qquad (3.1.1)$$
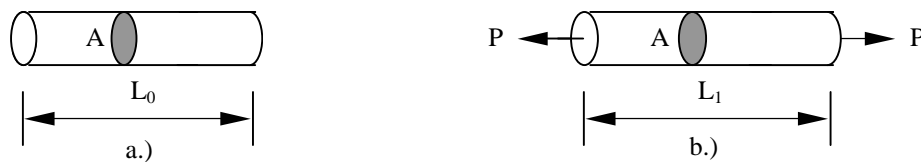


Fig. 3.1. A beam in tension a.) Before loading b.) After loading.

Normal axial strain is the elongation per unit length. The elongation of an object is the cumulative consequence of the deformation of all elements of the material throughout the volume of that object. For axial loading on a straight beam, the axial strain is

$$\varepsilon = \delta/L_0 \tag{3.1.2}$$

where $\varepsilon$ is stain, $\delta$ is the total elongation, and $L_0$ is the initial length. There are two types of normal strains, tensile and compressive, corresponding to the normal stress direction.

For a linearly elastic material, the modulus of elasticity (E) is the slope of the linear relationship between axial stress and axial strain for a uniaxially loaded specimen as shown in Fig. 3.1. This is expressed by the following equation

$$E = \sigma/\varepsilon \tag{3.1.3}$$

3.1.2. Bending Moments

When a positive bending moment is applied on the beam of Fig. 3.2, compressive bending stresses act above the neutral axis, while tensile stresses act below the neutral axis. In contrast, if the direction of the bending moment is reversed, i.e. a negative bending moment, all stresses will be reversed in Fig. 3.2. The neutral axis passes through the centroid of the cross-sectional area, e.g. the center point in a beam of circular shape. From elementary beam theory the magnitude of the stress is

$$\sigma_X = MY/I \tag{3.1.4}$$
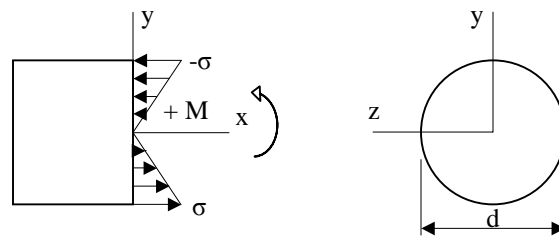


Fig. 3.2. a.) Relationship between bending moment and directions of normal stress in x-y plane b.) cross-sectional circular shape in y-z plane.

where $\sigma_x$ is normal stress, M is the bending moment, y is the distance from the neutral axis, and I is moment of inertia with respect to a horizontal line through the centroid. For a round cross-sectional area, the moment of inertia is

$$I = \pi d^2/4 \qquad\qquad (3.1.5)$$

where d is diameter of the beam as shown in Fig. 3.2.

3.1.3. Cellular Solid Models

One form of cellular solid model of a material is a structure made up of a large number of interconnected beams. When this structure is loaded, the resultant overall behavior is a function of the geometry of the beam and of the structure, and the material properties of the structure elements. This overall behavior can be characterized as the apparent modulus of the "material" represented by the structure.

When applying a uniformly distributed axial load, F, on top of an ideal beam cellular solid material (Fig.3.3), the normal stresses act on only the longitudinal beams. Therefore, the apparent modulus of such a cellular solid material depends on the cross-sectional-area fraction. The following equations show the cross-sectional-area fraction, $A_f$, and the apparent modulus, E, of this ideal cellular solid material.

$$A_f = \pi N_l d^2/4A \qquad\qquad (3.1.6)$$

and
$$E = A_f E_b \qquad\qquad (3.1.7)$$

where $N_l$ is number of beams in the longitudinal direction, d is longitudinal diameter of each beam, A is overall cross-sectional area of the cellular structure, and $E_b$ is the beam modulus. In addition, the yield strength of this cellular solid structure depends only on the yield strength of the beams in the longitudinal direction.
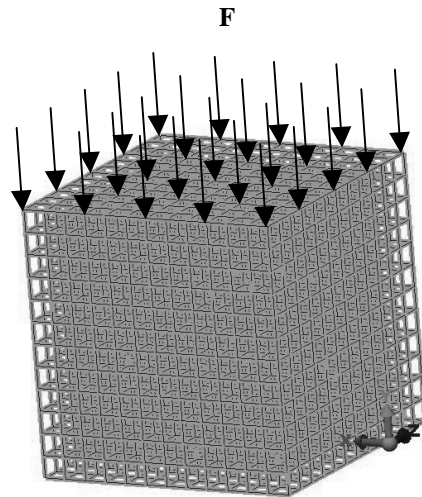
Fig. 3.3. An ideal cellular solid material with a distributed load.

With loading of a cellular solid material with a variation of beam lengths and orientations, stresses derive from axial stresses as well as bending moments on the beams in both the transverse and longitudinal directions. As shown in Fig. 3.4, the stress at any point of the beam can be compressive or tensile, depending on the combined effect of axial stress and bending moments. Therefore, the greatest stress at any point on the beam is the highest value at that point, derived from the combination of the stress from axial load and the stress from the bending moment. An individual beam will yield when the highest stress on any point of beam reaches the beam material's yield strength. The apparent modulus and strength of the overall cellular structure will vary with the cellular architecture (beam length and orientation), distributions (translating in part into apparent density), and component mechanical properties.
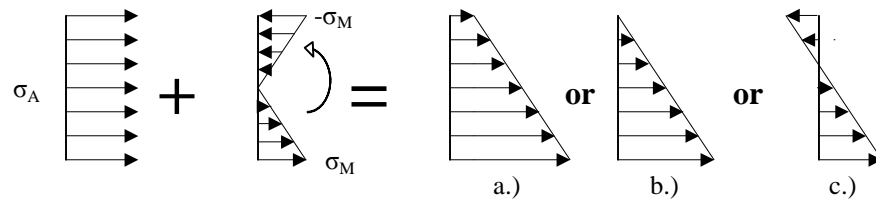
Fig. 3.4. A combination between axial stress, $\sigma_A$, and stresses from bending moment, $\sigma_M$.
a.) if $\sigma_A > |-\sigma_M|$. b.) if $\sigma_A = |-\sigma_M|$. c.) if $\sigma_A < |-\sigma_M|$. Therefore, the worst stress in this case is $\sigma_A + \sigma_M$.
Moreover, if $\sigma_A$ is only reversed, the stresses of a.), b.), and c.) will be reversed.

## 3.2 COMPOSITE MATERIAL

When a composite material such as that shown in Fig. 3.5 is uniaxially compressed, the two components must have equal strain assuming the top plate moves down while remaining horizontal. The following equilibrium equation can be used to find the compressive force in the two materials as fractions of the total load.

$$F_t = F_1 + F_2 \qquad\qquad (3.2.1)$$
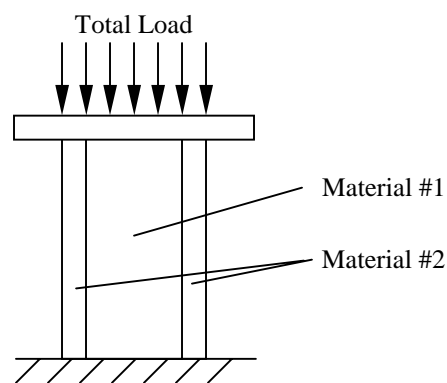


Fig. 3.5. A distributed load on two composite materials.

where $F_t$ is the total load on the two materials, and $F_1$ and $F_2$ are the loads on material #1

and #2, respectively. With substituting equation 3.1.1 into equation 3.2.1,

$$F_t = \sigma A = \sigma_1 A_1 + \sigma_2 A_2. \tag{3.2.2}$$

The overall area of the composite material, A, equals the summation of the cross-

sectional area of material #1 and cross-sectional area of material #2. The strains of the

two materials, $\varepsilon_1$ and $\varepsilon_2$, are equal because both have the same displacement and same

length. Therefore, from equation 3.1.1 and 3.2.2

$$E = E_1 A_{f1} + E_2 A_{f2} \tag{3.2.3}$$

where E is the overall or apparent modulus of the composite material and $A_{f1}$ and $A_{f2}$ are

the cross-sectional area fraction of material #1 ($A_1/A$) and #2 ($A_2/A$), respectively.

The strength of the composite is a function of the relative areas of each as well

their moduli and individual strengths. As the overall load increases, the stress will reach

the ultimate stress of one of the materials before the other, assuming these ultimate

stresses are unequal. At this point the material whose ultimate stress has been reached

will undergo compressive failure. Its subsequent ability to carry load will then depend on

the nature of the failure and the geometric constrains.

Thus, the compressive failure of the composite can be a two-stage process in

which one material fails, with the other continuing to carry load until it also fails; or a

single stage process in which the failure of the first material immediately precipitates a

failure in the second. The first case may be recognizable by a jump or cusp in the overall

modulus from the stress-strain curve while the second case will reflect overall failure at

that load.

Finally, a cellular solid material consisting of two materials could also be considered a composite material, ignoring its far more complex structural details. The apparent modulus of a cellular solid material could then be estimated from equation 3.2.3.

## CHAPTER IV

## MODELING FOR TRABECULAR BONE

The model considered here is composed of rods (beams) linked as a non-uniform cubic network to represent "intact" trabecular bone (Fig. 4.1a). As in the idealized model of Jensen et al and Yeh et al (11,26), the trabeculae length in the transverse direction is shorter than the trabeculae length in the longitudinal direction. The ideal trabecular dimensions of 25, 60 and 80-year-olds from Table 4.1 were constructed by following the trabecular geometry equations of Yeh. In addition, from Table 4.1 the architectures were altered by flipping the lengths between transverse and longitudinal directions, while not changing the trabecular diameters in either direction. Unlike the perturbing model methods of Jensen and Yeh et al, have the ideal coordinates of a unit cell was perturbed by 5% and 10% coefficients of variation (COV) of trabeculae lengths and orientations. The ideal rectangular coordinates $(x,y,z)$ were transformed into spherical coordinate $(r,\theta,\varphi)$. The magnitudes of each $r$, $\theta$, and $\varphi$ were randomly drawn from their distributions of 5% and 10% COV. The varied spherical coordinates were converted back to rectangular coordinates. From average trabecular length ($L_t$ and $L_l$) in the transverse and longitudinal direction, the transformed coordinates of $(x,y,z)$ were obtained by adding terms of $mL_t/2$, $nL_t/2$ and $oL_l/2$ to x, y, and z, respectively, where m, n and, o are a series of numbers $-1, 1, 3, 5,\ldots, m_0, n_0$ and $o_0$. The trabecular rods were linked from those actual coordinates, and the apparent density of the "intact" model was calculated.

Trabecular diameters of both transverse and longitudinal directions were maintained for each model.

Table 4.1. Ideal rectangular lattice of trabecular bone models in three dimensions with round trabeculae,
where $L_t$, $L_l$: Trabecular lengths in transverse and longitudinal directions, respectively
BV, TV: Bone volume and total volume, respectively
$d_t$, $d_l$: Trabecular diameters in transverse and longitudinal directions, respectively

| Age (years) | Trabeculae dimension | | | | | |
|---|---|---|---|---|---|---|
| | $L_t$ ($\mu$m) | $L_l$ ($\mu$m) | BV (cm$^3$) | TV (cm$^3$) | $d_t$ ($\mu$m) | $d_l$ ($\mu$m) |
| 25 | 624 | 631 | 0.09 | 0.42 | 164 | 215 |
| | 631 | 624 | 0.09 | 0.43 | | |
| 60 | 858 | 1110 | 0.04 | 0.46 | 129 | 215 |
| | 1110 | 858 | 0.03 | 0.47 | | |
| 80 | 992 | 1384 | 0.03 | 0.52 | 109 | 215 |
| | 1384 | 992 | 0.02 | 0.55 | | |

Before testing the "intact" bone models, three different types of boundary conditions were used on the "intact" 25-year-old model with longer transverse trabeculae to check the effect of boundary conditions on the behavior of the trabecular bone model. The first boundary condition was with the bottom fixed with respect to both translation and rotation, and the top fixed with respect to rotation and X, Y translation, but with translation allowed in the Z direction. The second boundary condition was with the bottom fixed with respect to both rotation and translation, the top fixed for X, Y translation, and with Z translation and free rotation allowed. The third boundary condition was with the bottom fixed with respect to X and Y rotation, and Z translation, and X, Y translation only at the X-axis and Y-axis, respectively. The top was fixed with respect to Z rotation, with the remaining translations and rotations on the top and bottom allowed. These cases are shown in Table 4.2.

Table 4.2. Three types of boundary conditions were used on the intact bone model with longer transverse trabeculae

| | 1st boundary condition | | 2nd boundary condition | | 3rd boundary condition | |
|---|---|---|---|---|---|---|
| | Rotation | Translation | Rotation | Translation | Rotation | Translation |
| At the bottom | Fixed | Fixed | Fixed | Fixed | Z Free X,Y Fixed | Z Fixed X,Y Fixed only at Y- and X-axis, respectively, The rest Free |
| On the top | Fixed | Z Free X,Y Fixed | Free | Z Free X,Y Fixed | Z Free X,Y Fixed | Free |

"Damaged" bone models were created by randomly removing trabeculae from the "intact" 25-year-old model with longer transverse trabeculae and 5%COV. The 5% and 10% decrease of bone volumes were applied in both the transverse and longitude directions. In addition, the combination of removing both transverse and longitudinal trabeculae to a total of 10% and 15% were built from the 5% and 10% decreases.

For this study using the intact 25-year-old model with 5% COV and longer transverse trabeculae, trabeculae with stresses greater than 90% of maximum were intentionally removed at the end each simulation. This was intended to simulate progressive damage based on highest stresses. This is distinguished from the other damage models, which based on random trabeculae removal. Finally, bone volume of overall removing trabeculae at the 30th simulation was determined and the overall mechanical properties at this point were compared with the mechanical properties of other damage models. This process appeared to result in progressive failure rather the reaching a plateau.

In addition, the "intact" 80-year-old model with longer longitudinal trabeculae and 5%COV was constructed as a columnar elliptical shape of 6.5 by 7.5 cm$^2$ and 8.3 mm of height as shown in Fig. 4.1 b.) and c.).
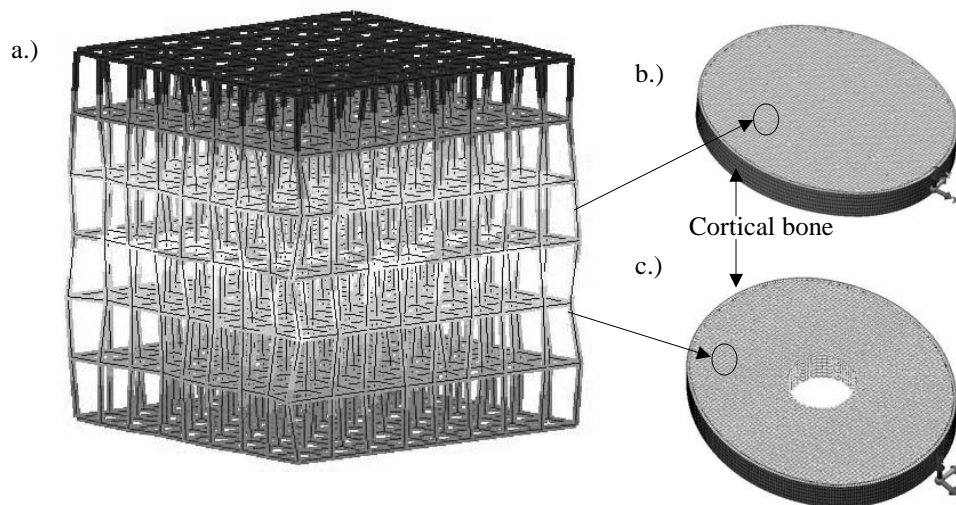


Fig 4.1.  a.) An "intact" trabecular bone model with variation of lengths and orientations.
b.) and c.) A slice of bone that contains an "intact" trabecular bone model and an cortical bone sheet model with a tray loading on top of model with b.) stem-less and c.) stem.

A first model like indentation test was simulated with the same "platen" size as that of the previous "intact" simulation. Second and third models, simulated the tibial tray of a knee prosthesis, without and with stem, respectively. Moreover, with considering trabecular bone as a solid material covered by a cortical shell, the second model was evaluated as a simple composite model of two materials.

In the models, the mechanical properties of trabeculae were estimated from properties of cortical bone. A linearly elastic, isotropic material was assumed for each trabecula with a Poisson's ratio of 0.3, a trabeculae modulus of 12 GN/m$^2$, and a density of 1.8 kg/m$^3$. The shape of each trabecula is considered a perfect cylinder. A

compressive distributed axial load, 1 N/m$^2$ on top of the model was applied for every simulation. Following the analysis of the effect of boundary conditions, displacement and rotation boundary conditions were fixed in all directions at the bottom of all models. The apparent moduli of the trabecular models were calculated from the ratio of distributed load to normal strain in the longitudinal direction. The normal strains and the "worst" (highest) stresses were obtained through a finite element analysis program (ALGOR FEMPRO 14.202.2004; ALGOR, Inc. Pittsburgh, PA).

# CHAPTER V

# RESULTS

## 5.1. INTACT TRABECULAR BONE MODELS

The effects of boundary condition are shown in Tables 5.1 and 5.2. The effect is less than 5%, respectively except for the greatest tensile stress for which some are higher than 5%. Based on these results the first boundary condition was applied to the rest of the trabecular bone models studied.

When the architecture of the trabecular models in terms of age was changed with increasing lengths and decreasing diameters of trabeculae, the apparent modulus was decreased and the worst stresses in the trabeculae were increased (Table 5.3 and Fig.

Table 5.1. Effect of boundary condition on highest worst stress on trabeculae of 25-year-old model with longer transverse trabecular

| Highest worst stress ($N/m^2$) | Ideal column (Percent difference*) | | 5% COV (Percent difference*) | | 10% COV (Percent difference*) | |
|---|---|---|---|---|---|---|
| | Tension | Compression | Tension | Compression | Tension | Compression |
| First boundary condition | 0.04 | 10.4 | 19.8 | 32.0 | 34.8 | 59.1 |
| Second boundary condition | 0.03 (25.0%) | 10.4 (0.0%) | 19.8 (0.0%) | 32.0 (0.0%) | 34.8 (0.0%) | 59.1 (0.0%) |
| Third boundary condition | 0.19 (78.9%) | 10.5 (1.2%) | 19.5 (1.8%) | 31.9 (0.4%) | 40.8 (17.2%) | 61.5 (4.0%) |

 * Comparing with first boundary condition in absolute value

Table 5.2. Effect of boundary condition on apparent modulus of 25-year-old model with longer transverse trabecular

| Axial apparent modulus ($N/m^2$) | Ideal column (Percent difference*) | 5% COV (Percent difference*) | 10% COV (Percent difference*) |
|---|---|---|---|
| First boundary condition | $1.2 \times 10^9$ | $1.1 \times 10^9$ | $8.6 \times 10^8$ |
| Second boundary condition | $1.2 \times 10^9$ (0.0%) | $1.1 \times 10^9$ (0.0%) | $8.5 \times 10^8$ (0.2%) |
| Third boundary condition | $1.2 \times 10^9$ (0.0%) | $1.0 \times 10^9$ (9.1%) | $8.4 \times 10^8$ (2.3%) |

 * Comparing with first boundary condition in absolute value

Table 5.3. Comparison of 3 models at different age with first boundary conditions at a.) Ideal column b.) 5%COV and c.) 10%COV

a.)

| **Longitudinal trabeculae are longer** | | 25 year old | 60 year old | 80 year old |
|---|---|---|---|---|
| Highest worst stress of (N/m$^2$) | Tension | 0.55 | 0.04 | 0.34 |
| | Compression | 10.1 | 18.2 | 23.6 |
| In Z direction, the Maximum of | Displacement (m) | -6.4x10$^{-12}$ | -1.2x10$^{-11}$ | -1.6x10$^{-11}$ |
| | Strain (m/m) | -8.5x10$^{-10}$ | -1.5x10$^{-9}$ | -2.0x10$^{-9}$ |
| | Apparent modulus (N/m$^2$) | 1.2x10$^9$ | 6.6x10$^8$ | 5.1x10$^8$ |
| **Transverse trabeculae are longer** | | 25 year old | 60 year old | 80 year old |
| Highest worst stress of (N/m$^2$) | Tension | 0.04 | 0.04 | 0.02 |
| | Compression | 10.4 | 28.8 | 42.3 |
| In Z direction, the Maximum of | Displacement (m) | -6.5x10$^{-12}$ | -1.9x10$^{-11}$ | -2.8x10$^{-11}$ |
| | Strain (m/m) | -8.6x10$^{-10}$ | -2.6x10$^{-9}$ | -3.6x10$^{-9}$ |
| | Apparent modulus (N/m$^2$) | 1.2x10$^9$ | 3.9x10$^8$ | 2.8x10$^8$ |

b.)

| **Longitudinal trabeculae are longer** | | 25 year old | 60 year old | 80 year old |
|---|---|---|---|---|
| Highest worst stress of (N/m$^2$) | Tension | 9.84 | 29.3 | 42.9 |
| | Compression | 23.7 | 48.8 | 69.6 |
| In Z direction, the Maximum of | Displacement (m) | -6.7x10$^{-12}$ | -1.2x10$^{-11}$ | -1.8x10$^{-11}$ |
| | Strain (m/m) | -8.8x10$^{-10}$ | -1.6x10$^{-9}$ | -2.1x10$^{-9}$ |
| | Apparent modulus (N/m$^2$) | 1.1x10$^9$ | 6.3x10$^8$ | 4.7x10$^8$ |
| **Transverse trabeculae are longer** | | 25 year old | 60 year old | 80 year old |
| Highest worst stress of (N/m$^2$) | Tension | 19.82 | 56.5 | 105.7 |
| | Compression | 32.02 | 101.3 | 192.9 |
| In Z direction, the Maximum of | Displacement (m) | -7.12x10$^{-12}$ | -2.12x10$^{-11}$ | -3.16x10$^{-11}$ |
| | Strain (m/m) | -9.51x10$^{-10}$ | -2.94x10$^{-9}$ | -3.98x10$^{-9}$ |
| | Apparent modulus (N/m$^2$) | 1.05x10$^9$ | 3.41x10$^8$ | 2.52x10$^8$ |

c.)

| **Longitudinal trabeculae are longer** | | 25 year old | 60 year old | 80 year old |
|---|---|---|---|---|
| Highest worst stress of (N/m$^2$) | Tension | 22.1 | 80.2 | 109 |
| | Compression | 33.6 | 153 | 175 |
| In Z direction, the Maximum of | Displacement (m) | -7.5x10$^{-12}$ | -1.4x10$^{-11}$ | -2.1x10$^{-11}$ |
| | Strain (m/m) | -9.9x10$^{-10}$ | -1.8x10$^{-9}$ | -2.5x10$^{-9}$ |
| | Apparent modulus (N/m$^2$) | 1.0x10$^9$ | 5.5x10$^8$ | 4.0x10$^8$ |
| **Transverse trabeculae are longer** | | 25 year old | 60 year old | 80 year old |
| Highest worst stress of (N/m$^2$) | Tension | 34.8 | 76.0 | 233 |
| | Compression | 59.1 | 263 | 348 |
| In Z direction, the Maximum of | Displacement (m) | -8.8x10$^{-12}$ | -2.7x10$^{-11}$ | -5.3x10$^{-11}$ |
| | Strain (m/m) | -1.2x10$^{-9}$ | -3.7x10$^{-9}$ | -6.7x10$^{-9}$ |
| | Apparent modulus (N/m$^2$) | 8.6x10$^8$ | 2.7x10$^8$ | 1.5x10$^8$ |

5.1). As shown in Fig. 5.1 a.) and b.), even though the change of standard deviation of trabeculae length and orientation was of 5% and 10%, there is a dramatic influence on the worst stress on the trabeculae. Notably, the highest worst stresses with high trabecular space as in 80-year-old people at 10%COV are about 300-fold and 7-fold higher compared with a perfect columnar trabecular bone for tensile and compressive stress, respectively, when longitudinal trabeculae are longer. When transverse trabeculae are longer these stress are about 10000-fold and 8-fold for tensile and compressive stress, respectively. Moreover, all models showed that the longitudinal trabeculae were under compressive worst stresses, but transverse trabeculae were under both tensile and compressive worst stresses. The results further predict that trabeculae would yield (or fail) at both ends where they are connected to other surrounding trabeculae.

Tables 5.3, and Fig. 5.1 to 5.3 also show the apparent modulus calculated from the displacement in the Z direction. From Fig. 5.2 the normalized apparent modulus compared with each ideal model is seen to decrease when increasing the distribution of trabeculae lengths and orientations. When trabecular space was increased, the apparent modulus with the longer trabeculae length in the transverse direction was decreased more than the apparent modulus with the longer trabeculae length in the longitudinal direction.

From Fig. 5.3, with both longer transverse and longer longitudinal trabeculae, the ratio of the apparent modulus to the trabeculae modulus for the younger bone are higher than for the older bone. In addition the relationships between the ratio of apparent modulus to trabeculae modulus and the ratio of bone volume to total volume (BV/TV)

Highest worst stress on
trabeculae (N/m$^2$)

Highest worst stress on
trabeculae (N/m$^2$)

a.)

b.)
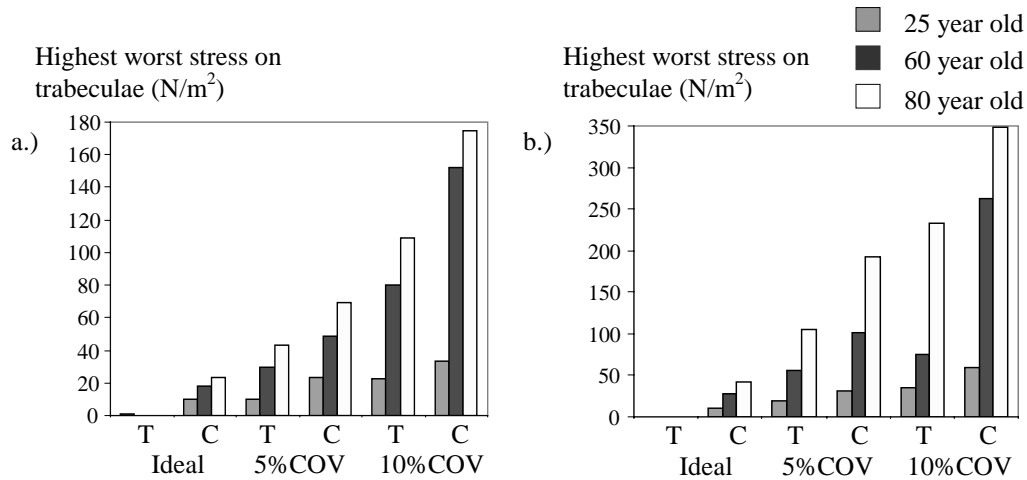
Fig. 5.1. The maximum of worst stress in tension (T) and compression (C) by varying the COV of trabeculae lengths and orientations from ideal columnar trabecular bone model at 25, 60 and 80 year old model when a.) trabeculae in the longitudinal direction are longer and b.) trabeculae in the transverse direction are longer.

Normalized apparent
modulus (N/m$^2$)/(N/m$^2$)
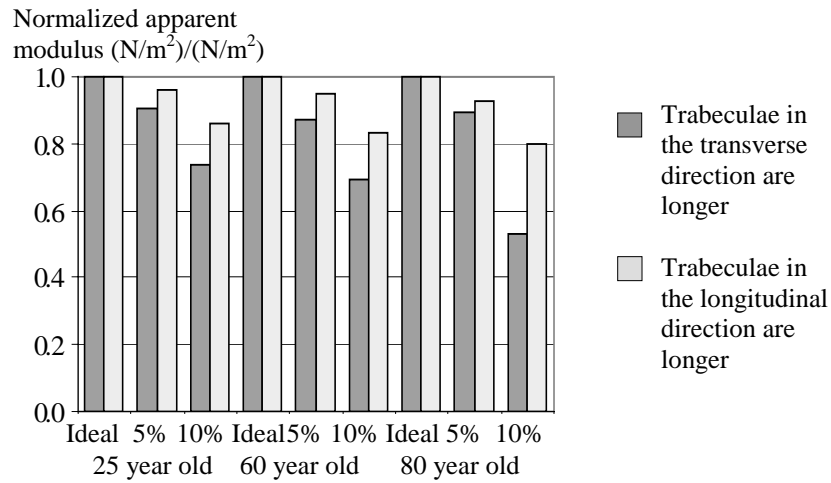
Fig. 5.2. The relationship between age and relative apparent modulus by 5% and 10% variation of lengths and orientation from ideal columnar trabecular bone model.

are linear with a high correlation coefficient, r$^2$ (higher than 0.994). However, the ratio of apparent modulus to trabeculae modulus in the case of the longer transverse trabeculae is lower than the ratio of apparent modulus to trabeculae modulus in the case

Relative apparent modulus
(N/m$^2$)/(N/m$^2$)

Transverse trabeculae are longer

--- Longitudinal trabeculae are longer



Ideal Model
$Y_{ideal} = 0.47x$,
$r^2 = 0.996$

5% COV
$Y_{5\%COV} = 0.43x$,
$r^2 = 0.994$

10%COV
$Y_{10\%COV} = 0.37x$,
$r^2 = 1.000$

Ideal Model
$Y_{ideal} = 0.40x+0.02$,
$r^2 = 0.998$

5% COV
$Y_{5\%COV} = 0.39x+0.02$,
$r^2 = 0.997$

10%COV
$Y_{10\%COV} = 0.36x+0.01$,
$r^2 = 0.997$
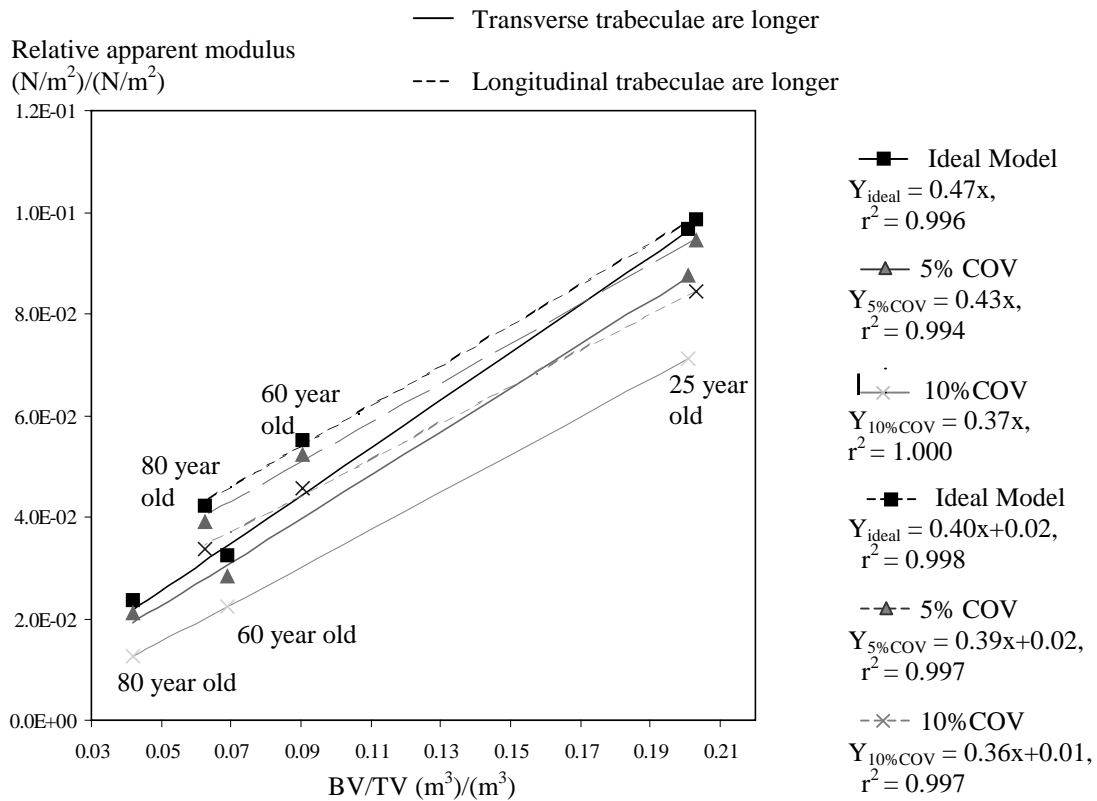
Fig. 5.3. The relationship between relative apparent modulus and BV/TV by varying the variation of lengths and orientation from ideal columnar trabecular bone model.

of the longer longitudinal trabeculae. Moreover, increasing %COV in both cases of the longer trabeculae lengths also influenced the decrease of apparent bone modulus and increase of worst stresses on the trabeculae.

5.2. DAMAGED TRABECULAR BONE MODELS

Using the intact 25-year-old with 5% COV and longer transverse trabeculae model, when the architecture of the trabecular models were changed by decreasing BV by removing trabeculae from intact trabecular bone, the worst stresses of tension and compression in the trabeculae were increased. These stresses were more increase more by removing trabeculae in the longitudinal direction (Table 5.4). In addition, Tables 5.3

Table 5.4. Mechanical properties of trabecular model with varying missing trabeculae at 25-year-old model, 5%COV, and longer transverse trabeculae of a.) separation in the transverse and longitudinal directions, and b.) combination in the transverse and longitudinal directions

a.)

| | | Amount of Missing Trabecular Bone in | | | |
|---|---|---|---|---|---|
| | | Transverse direction | | Longitudinal direction | |
| | | 5% BV | 10% BV | 5% BV | 10% BV |
| Highest of worst stress of (N/m$^{2)}$ | Tension | 22.0 | 29.1 | 95.8 | 178 |
| | Compression | 42.5 | 43.6 | 114 | 175 |
| In Z direction, the maximum of | Displacement (m) | $-7.3 \times 10^{-12}$ | $-7.5 \times 10^{-12}$ | $-1.4 \times 10^{-11}$ | $-2.7 \times 10^{-11}$ |
| | Strain (m/m) | $-9.7 \times 10^{-10}$ | $-1.0 \times 10^{-9}$ | $-1.9 \times 10^{-9}$ | $-3.6 \times 10^{-9}$ |
| | Apparent modulus (N/m$^2$) | $1.0 \times 10^{9}$ | $1.0 \times 10^{9}$ | $5.3 \times 10^{8}$ | $2.8 \times 10^{8}$ |

b.)

| | | Amount of Missing Trabecular Bone in | | | |
|---|---|---|---|---|---|
| | | Longitudinal direction w/5% BV missing in transverse direction | | Transverse direction w/5% BV missing longitudinal direction | |
| | | 5% BV | 10% BV | 5% BV | 10% BV |
| Highest of worst Stress of (N/m$^{2)}$ | Tension | 106 | 104 | 106 | 199 |
| | Compression | 116 | 125 | 116 | 195 |
| In Z direction, the maximum of | Displacement (m) | $-1.5 \times 10^{-11}$ | $-1.2 \times 10^{-11}$ | $-1.5 \times 10^{-11}$ | $-3.0 \times 10^{-11}$ |
| | Strain (m/m) | $-2.0 \times 10^{-9}$ | $-2.2 \times 10^{-9}$ | $-2.0 \times 10^{-9}$ | $-4.0 \times 10^{-9}$ |
| | Apparent modulus (N/m$^2$) | $5.0 \times 10^{8}$ | $4.6 \times 10^{8}$ | $5.0 \times 10^{8}$ | $2.5 \times 10^{8}$ |

and Fig. 5.4 and 5.5 show the apparent modulus calculated from the displacement in the Z direction. From Fig. 5.4, missing some trabeculae in the transverse direction decreased the apparent modulus much less than missing trabeculae in the longitudinal direction at the same amount of bone volume. It was also found that the quantity missing in the longitudinal direction has greater influence on the worst stresses both in tension and compression. From regression analysis there is a linear relationship when removing trabeculae in the transverse direction with fixed amount of trabecular in the longitudinal direction. However, there is an exponential relationship with increasing trabeculae loss in the longitudinal direction and fixed amount of trabecular in the transverse direction.

Apparent modulus (N/m$^2$)
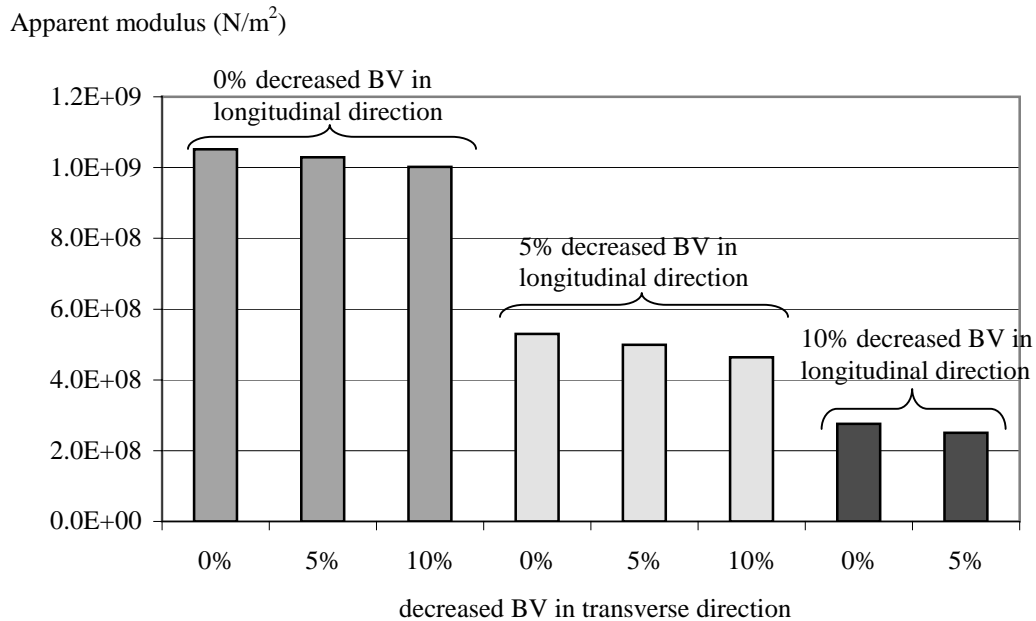


Fig. 5.4. The relationship between apparent and modulus decreasing percent of BV by removing trabeculae at 25-year-old model, 5%COV, and longer transverse trabeculae.

As shown in Fig. 5.5, at 0% and 5% BV missing in the transverse direction the ratio of apparent modulus to trabeculae modulus is linearly related to BV/TV with a slope of 0.21 and 0.27, respectively. However, at 0% and 5% BV missing trabeculae in the longitudinal direction the ratio of apparent modulus to trabeculae modulus is related to an exponential of BV/TV multiplied by 66.6 and 70.4, respectively. Therefore, the upper boundary of the relationship of the ratio of apparent modulus to trabeculae modulus and BV/TV is only from missing bone in the transverse direction and the lower boundary of the relationship of the ratio of apparent modulus to trabeculae modulus and BV/TV is from missing bone volume in the longitudinal direction. It should be noted here that the loss in apparent density of the longitudinal and transverse trabeculae missing models are the same, yet the effect on modulus and strength are very different.

Relative apparent modulus
$(N/m^2)/(N/m^2)$
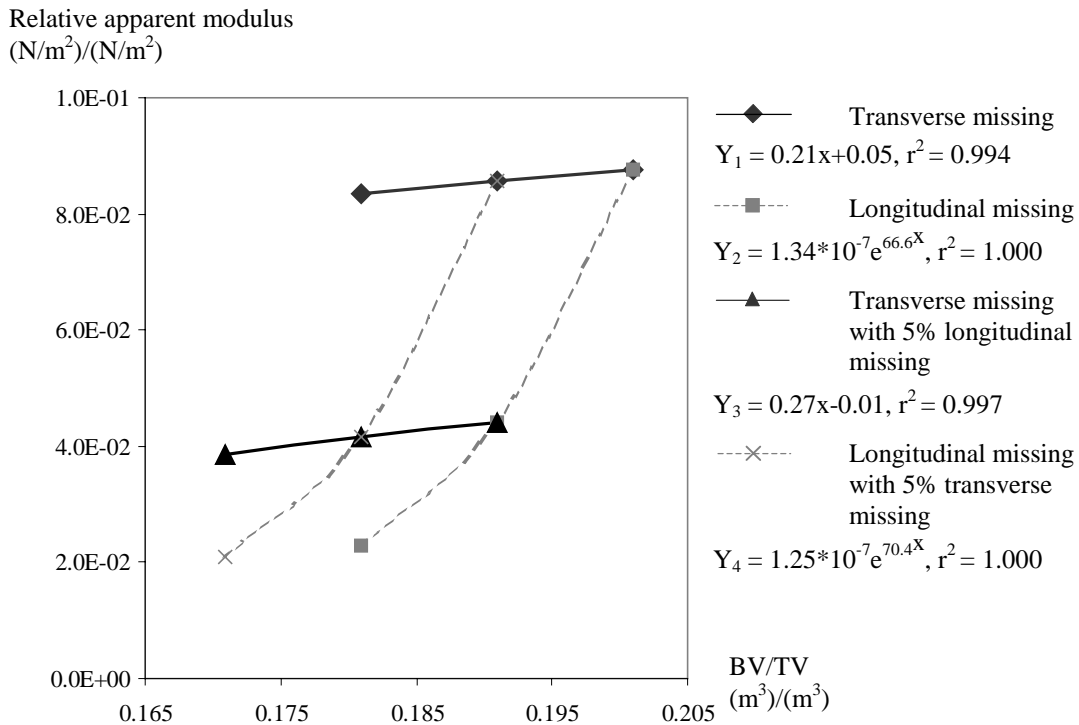


Fig. 5.5. After removing some of trabeculae the relationship between the ratio of apparent modulus to trabeculae modulus and BV/TV at 25-year-old model, 5%COV, and longer transverse trabeculae.

Furthermore, the model result would be the same if trabeculae where considered broken or non-load bearing rather than missing". In this case BV would be the same as in the intact models, despite the loss of the modulus and strength. Therefore, BV is not itself a predictor of loss of mechanical properties.

In the final step of the stepwise removal simulation, 42 and 62 trabeculae were removed in the longitudinal and the transverse directions, respectively from original model. Therefore, intact trabecular bone volumes in the longitudinal and transverse directions were decreased to 99.37% and 99.13%, respectively. Overall displacement in the axial direction in the last simulation was $8.7 \times 10^{-12}$ m. Therefore, the overall apparent

modulus was $8.6 \times 10^8$ N/m$^2$. For the highest worst stresses both tension and compression varied between 25 and 55 N/m$^2$. However, the trend of worst stresses increased overtime. Trabeculae in the longitudinal direction failed first, followed by the some of trabeculae in the transverse direction. Trabeculae in the longitudinal direction failed because of compressive worst stresses, but trabeculae in the transverse direction failed because of both tensile and compressive worst stresses. Moreover, the subsequently removed trabeculae were mostly near the previous removed trabeculae.

## 5.3. TRABECULAR BONE WITH CORTICAL BONE MODELS

With the same size of plate (referring to Table 5.3.b) loading on trabecular bone with and without cortical bone, the apparent modulus of a plate loaded specimen of trabecular bone with a cortical bone shell for the 80-year-old with 5%COV, and longer longitudinal trabeculae is $4.9 \times 10^8$ N/m$^2$, which is 3.7% higher than the apparent modulus of trabecular bone without cortical bone. It is noteworthy that the highest stresses in both tension and compression were increased about 45% and 25%, respectively as shown in Table 5.5. However, the highest stresses mostly appeared near the loading plate instead of being randomly distributed. The reason for this is that the nearest trabeculae, which connect to the loaded trabecular under the loading plate are constrained in displacement, thus increasing the overall apparent modulus from reduction of the displacement, but the side surface of the trabecular model without cortical is unconstrained. This model also showed that the transverse trabeculae were under the worst stresses in both tension and compression, but the longitudinal trabeculae were mostly under the worst stresses in compression.

Table 5.5. Comparing the mechanical properties of trabecular between with and without cortical bone by using the same size of loaded plate of 80-year-old model (referring from Table 5.3.b) with 5%COV and longitudinal trabeculae are longer

|  |  | With cortical | W/o cortical* |
|---|---|---|---|
| Highest stress of (N/m²) | Tension | 62.2 | 42.9 |
|  | Compression | 87.2 | 69.6 |
| In Z direction, the Maximum of | Displacement (m) | $-1.7 \times 10^{-11}$ | $-1.8 \times 10^{-11}$ |
|  | Strain (m/m) | $-2.0 \times 10^{-9}$ | $-2.1 \times 10^{-9}$ |
|  | Apparent modulus (N/m²) | $4.9 \times 10^{8}$ | $4.7 \times 10^{8}$ |

* Referring to Table 5.3.b.)

Table 5.6. The apparent modulus of sliced bone which comparing between the results from an FEA program, and calculating as a composite material by assuming the modulus of cortical bone is $1.2 \times 10^{10}$ N/m² and using result from 80 year old model the modulus of trabecular bone is $4.7 \times 10^{8}$ N/m²

| Axial apparent modulus (N/m²) | Stem-less with considering trabecular bone model as (Percent difference*) | | 1.8 cm diameter stem (Percent difference**) |
|---|---|---|---|
|  | A trabeculae network | A solid material |  |
| A composite material† | 1.12x10⁹ | | 1.09x10⁹ |
| From lowest displacement of a tibial tray‡ | 1.13x10⁹ (0.63%) | 1.33x10⁹ (18.8%) | 1.03x10⁹ (5.15%) |
| From highest displacement of a tibial tray‡ | 8.95x10⁸ (19.9%) | 1.07x10⁹ (4.46%) | 7.74x10⁸ (28.8%) |

* Comparing the modulus of stem-less model between FEA results and composite material results in absolute value
** Comparing the modulus of stem model between FEA results and composite material results in absolute value
† Calculated from summation of cross-sectional area fraction multiplied by its own material's modulus [Eq. 3.2.3]
‡ Measuring displacement at the top of sliced bone

The whole slice bone models in Fig. 4.1 b.) and c.) were used to compare the overall mechanical properties and interactions between stem and stem-less tibial trays of knee prostheses. As mentioned, the mechanical properties of cortical bone have been assumed to be the same as trabeculae mechanical properties. As shown in Table 5.6, the overall apparent bone modulus with both stem and stem-less tray models, calculated from highest displacements, were increased about 39.2 and 47.5%, respectively when compared to the apparent modulus of trabecular bone model. In comparison between

stem and stem-less tray models, 7% decrease of the area of trabecular bone because of the tray stem, the overall apparent modulus of the sliced bone model is decreased 13.6%. After applying a distributed load on top of the sliced bone in Fig. 4.1 b.) and c.), the deformations of both tray models are higher in the middle of the bone and lower at the cortical bone. Percent differences between highest and lowest displacements of stem-less and stem are about 20.4% and 24.9%, respectively. In both sliced bone models the worst trabeculae stresses in the transverse direction were tension and compression and in the longitudinal direction were only compression. Moreover, by assuming that the stem moves freely without any constrain, the highest worst stress of the stem tray model took place entirely at the stem's surface. Therefore, the sliced bone model with stem predicts failure first at the connecting surface of the stem. For a porous stem the boundary condition at the stem surface would presumably change over time from unconstrained to some degree of constraint.

Assuming the entire trabeculae area as solid trabecular bone, the sliced bone could be considered as a composite material composed of trabecular bone and cortical bone. With dimensions of the sliced bone, the relative loaded areas of trabecular and cortical bone are 94.4% and 5.6% of total loaded area, $3.8 \times 10^{-3}$ $m^2$, respectively. The modulus from the composite material is the summation of cross-sectional area fraction multiplied by modulus of each part as shown in Eq. 3.2.3. That equation assumes no Poisson's ratio effect. With a 1.8 cm diameter tray stem, the relative loaded area of trabecular bone was decreased to 87.8%. Therefore, the apparent modulus of the sliced bone as a composite material was decreased as shown in Table 5.6. Finally, when

comparing the apparent modulus that resulted from the FEA program to the apparent modulus calculated by using composite material assumptions, at lowest displacement the percent differences were 0.6% and 5.2% from the stem and stem-less model, respectively, while at highest displacement the percent differences were 19.9% and 28.8% from the stem and stem-less model, respectively.

With applying Poisson's ratio of 0.3 and apparent modulus of $4.7 \times 10^8$ N/m$^2$ on trabecular bone, a simple composite of two materials like Fig. 3.5 was analyzed by the FEA program. The results show (Table 5.6) that the overall modulus comparing with result from Eq. 3.2.3 was higher by about 19% from lowest displacement and was lower by about 5% from highest displacement. Using solid trabecular bone in the simple composite model ignores its porosity and therefore gives greater stiffness. The composite model could perhaps be improved by reducing the effective area of the trabecular bone. Comparison with the FEA model suggests an effective area of about 85% as shown in Table 5.6.

**CHAPTER VI**

**DISCUSSION AND CONCLUSIONS**

This study shows how the variation of trabeculae lengths and orientations in an ideal model and how the trabecular space, i.e. apparent density, which mostly depends on age and disease, effects the apparent modulus. Similarly, the calculation of trabeculae with highest stresses, which would yield under sufficient load, suggests a propagating failure pattern reflected as overall strength. It is concluded that how low the apparent modulus is depends on both how high the geometric variation is, and how low the apparent density is. Therefore, neither bone volume nor apparent density is enough to determine the mechanical properties of trabecular bone since the trabecular architecture plays an important role in modulus and strength. The trabeculae length and percent of missing trabeculae in the longitudinal direction have much more influence on the trabecular modulus and strengths than does the trabeculae length and percent trabeculae missing in the transverse direction. Assuming a maximum normal stress failure model, trabeculae in the transverse and longitudinal directions would fail because of combined bending moment and axial load. However, the trabeculae in the longitudinal direction mostly undergo compressive stress, when an axial distributed load was applied. Therefore, the longitudinal trabeculae will reach the yield strength (or fail) after enough transverse trabeculae have failed because an increase in missing transverse trabeculae will increase trabeculae worst stresses in both directions.

The relationship between overall stress and strain is linear in the early stage of loading. When the worst stress on trabeculae is high enough the transverse trabeculae fail first. When transverse trabeculae fail, it is generally equivalent to bone volume missing in the transverse direction at the same level of longitudinal trabeculae as in Fig. 5.5. Therefore, the slope of the overall stress-strain relationship, i.e. apparent modulus, decreases a small amount compared to the original stage during transverse trabeculae failure. When enough broken trabeculae accumulate in the transverse direction, some of the longitudinal trabeculae would start to fail, decreasing the slope of the stress-strain relationship drastically. In the following stage, the failed trabeculae in both directions rapidly propagate, so the apparent modulus would approach zero until the trabecular bone becomes completely dense. Finally, the stress would then start to build up after densification, if all of the failed bone remains intact.

As mentioned earlier, this research used the ideal trabecular architecture from Yeh (26) and then varied the coordinates of the trabeculae joints to alter lengths and orientations of individual trabeculae. Yeh et al fixed at the one variation of lengths and orientations and only varied the trabeculae thickness instead and found that the relationships between the apparent modulus and BV/TV of each coefficient of variation of thickness were linear. Even though these relationships from our research were also linear (Fig. 5.3), the relative modulus was higher at the same amount of BV/TV. The reason for this is that variations of the trabeculae thickness in the longitudinal and transverse directions of this research are constant compared with Yeh's research. Therefore, it is expected that if the trabeculae diameters of Table 4.1 are varied like Yeh

did, the relative modulus at the same amount of BV/TV should also be decreased. These results illustrate once again that BV/TV is a far too imprecise measure of bone condition since widely varying architectural situations can have the same BV/TV yet significantly different mechanical behavior.

The trabecular models of Jensen (11) et al were constructed by varying the trabeculae lengths by using the "relative lattice disorder, α". Their results correspond to the results in Fig. 5.3 that show increasing variation of trabeculae lengths decreases the apparent modulus compared to the intact model. Moreover, Jensen found that the horizontal stiffness was lower than the longitudinal stiffness. This is similar to our results obtained after flipping the lengths between the transverse and longitudinal directions. With longer transverse trabeculae the apparent modulus was lower than the modulus with shorter transverse trabeculae. This supports the above statements that the longitudinal trabeculae play an important part in the trabecular modulus.

Unlike other 3D models from Jensen, Yeh and this present work, Kim et al (14)'s model is a hexagonal columnar structure with uniform and tapered trabeculae. However, Kim did not vary length, thickness, and orientation. Their mechanical results were used to find the relationship with age and sex "caused" by varied BV/TV. When comparing with our results, our relative modulus is much higher than Kim's either uniform or tapered trabeculae at same age. However, trends of those relationships are the same with the trabecular modulus decreased with age.

In the 2-D trabecular model, Silva et al (22) constructed a perturbed trabecular bone model and then also removed some trabeculae. They found that percent density

reduction influences the apparent modulus and strength. In comparison with our 3-D models of decreasing relative density with the 2-D models of Silva, the relationship of the relative modulus to BV/TV show a similar curve. Silva also addressed the direction of removed trabeculae; showing that eliminating transverse trabeculae decreased the modulus linearly, but removing longitudinal trabeculae decreased the modulus in an exponential or quadratic curve like Fig. 5.5. The boundaries of the relative apparent modulus to BV/TV relationship showed that the upper boundary is from missing trabeculae in only the transverse direction and the lower boundary is missing trabeculae in only the longitudinal direction. Unlike Silva's research, this research also modeled the combination of missing trabeculae in both the transverse and longitudinal directions and found that the relationship of the ratio of apparent modulus to trabeculae modulus and BV/TV fell between those boundaries in combination of missing bone volume in both directions as shown in Fig. 5.5. This "damaged" trabecular model will be more useful to predict the mechanical properties of actual trabecular bone because the bone architecture is changed either from mechanical or chemical activities, or from both, as a result of age, drug treatment or drug abuse, space flight or exercises, and diseases like osteoporosis.

The difference between the broken trabeculae after loading beyond the yield strength of trabeculae and the missing trabeculae is that the broken trabeculae still remain in the trabecular bone, i.e. the bone volume is unchanged, but the mechanical properties of broken trabeculae are considered to be the same as those of missing trabeculae. In addition, it is possible that after no load is applied, the bone cells will remodel the broken trabeculae more readily than missing trabeculae and thus change and

restore the bone architecture and bone volume more readily than missing trabeculae. This suggestion may also be of use in future research on remodeling or adaptation of trabecular bone.

When a distributed load was applied, trabeculae where assumed to fail at the highest worst stresses. Even though the broken trabeculae are remaining in trabecular bone after failure, they were considered as missing trabeculae. At the same amount of percent trabeculae missing in the longitudinal and transverse directions, the relative apparent modulus of the damaged model (Fig. 5.5) was higher than the relative modulus from intentionally removing high stress trabeculae. At the last simulation this difference was about 10%. The probable reason for this is that propagation of failed trabeculae mainly occurred adjacent to high stress trabecular, while random removal occurs from both high stress and low stress areas. Selective material removal in high stress will reduce the overall mechanical properties more compared with the mechanical properties of randomly missing trabeculae. This progressive and propagated failure is also consistent with observations of the potential for extended strain after initial yielding.

Unlike previous solutions of simulation models that considered the compressive stresses of trabecular bone as a whole, our results showed the highest of the "worst" stresses of individual trabeculae. This helps to understand where the trabeculae fail and how trabecular bone fails from the trabeculae level. Moreover, no previous trabecular model combined a cortical model to construct a more complete tibia.

From percent differences in lower displacement from Table 5.6, when composing trabecular bone with a cortical shell under the same distributed load as a composite

material, the cortical bone supports the tibia bone because the modulus of cortical bone is much higher than the modulus of trabecular bone. Without cortical bone the trabecular can sustain about half of the load or less. From Hogan et al's paper (8) the modulus results from mechanical compressive tests of either sham or ovariectomized groups on rat tibia showed that the modulus of a whole slice is higher than the modulus of reduced-platen compression corresponding to our models as shown in Table 5.5. Hogan et al showed that the modulus of sham groups was higher than ovariectomized groups because in the latter the trabecular part is decreased by losing some of the trabeculae. When compared with our models the decreasing of trabecular modulus from missing trabeculae (damaged models) should influence the decrease of the modulus of the whole slice of bone, comparing to Table 5.6, where bone is considered as a solid composite material. Therefore, the modulus of tibia bone can roughly be predicted from a composite material, calculating from the modulus of cortical bone and trabecular bone with its own volume fraction. For the tibial tray, even though the stem helps knee prosthesis anchoring and protects against tray sliding on the top of the cut trabecular bone, the stem reduces the cross-sectional area of the overall sliced bone, and thus decreases the overall apparent modulus. Consequently, some patients, who also have osteoporosis, high bone loss, or revision, may not be able to tolerate the effect of reducing cross-sectional area. Stem-less tibial trays may be preferred.

In conclusion, the apparent modulus and strength of trabecular bone depend on the architecture of trabeculae and on the apparent density of trabecular bone. The longitudinal trabeculae play a more important role with respect to the apparent modulus

and strength of trabecular bone than the transverse trabeculae. This result implies different apparent moduli and strength for the same density depending on the nature of the bone loss. However, the transverse trabeculae are predicted to fail before the longitudinal trabeculae. When combining trabecular bone with cortical bone, tibia bone functions as a composite material and the higher modulus of cortical bone will increase tibia modulus to almost twice that of trabecular modulus alone. Finally, where considering trabecular bone as a simple solid material, the overall modulus using the FEA program was about 85% of the overall modulus for the porous material with a hard shell.

# REFERENCES

1. American Academy of Orthopaedic Surgeons: Number of arthroplasties to increase dramatically *The American Academy of Orthopaedic Surgeons Bulletin*, 50:1, 2002

2. Bourrin S, Ammann P, Bonjour JP, Rizzoli R: Recovery of proximal tibia bone mineral density and strength, but not cancellous bone architecture, after long-term bisphosphonate or selective estrogen receptor modulator therapy in aged rats. *Bone* 30:195-200, 2002

3. Carter DR, Hayes WC: The compressive behavior of bone as a two-phase porous structure. *J Bone Joint Surg Am* 59:954-962, 1977

4. Cowin SC: *Bone Mechanics Handbook,* 2nd ed. New York, CRC Press, 2001

5. Gibson LJ: The mechanical behavior of cancellous bone. *J Biomech* 18:317-328, 1985

6. Gibson LJ, Ashby MF: *Cellular Solid: Structure and Properties* 2nd ed, pp 103,186,310. United Kingdom, Cambridge University Press, 1997

7. Gunaratne GH, Mohanty KK, Wilmalawasa SJ: A model of trabecular bone and application to osteoporosis. *Physica A* 315:98-104, 2002

8. Hogan HA, Ruhmann SP, Sampson HW: The mechanical properties of cancellous bone in the proximal tibia of ovariectomized rats. *J Bone Miner Res* 15:284-292, 2000

9. Hvid I, Bentzen SM, Linde F, Mosekilde L, Pongsoipetch B: X-ray quantitative computed tomography: the relations to physical properties of proximal tibial trabecular bone specimens. *J Biomech* 22:837-844, 1989

10. Jee WSS: The Skeletal Tissues. In: *Cell and Tissue Biology, A Textbook of Histology,* Ed by L Weiss. Urban and Schwarzenberg, Baltimore, 1998

11. Jensen KS, Mosekilde Lis, Mosekilde Leif: A model of vertebral trabecular bone architecture and its mechanical properties. *Bone* 11:417-423, 1990

12. Keaveny TM, Wachtel EF, Ford CM, Hayes WC: Differences between the tensile and compressive strength of bovine tibial trabecular bone depend on modulus. *J Biomech* 27:1137-1146, 1994

13. Keyak, JH, Lee IY, Skinner HB: Correlations between orthogonal mechanical properties and density of trabecular bone: use of different densitometric measures. *J Biomed Mater Res* 28:1329-1336, 1994

14. Kim HS, Al-Hassani STS: A morphological model of vertebral trabecular bone. *J Biomech* 35,1101-1114, 2002

15. Majumda S, Kothari M, Augat P, Newitt DC, Link TM, Lin JC, Lang T, Lu Y, Genant HK: High-resolution magnetic resonance image: three dimensional trabecular bone architecture and biomedical properties. *Bone* 22:445-454, 1998

16. Mashiba T, Turner CH, Hirano T, Forwood MR, Jacob DS, Johnston CC, Burr DB: Effects of high-dose etidronate treatment on microdamage accumulation and biomechanical properties in beagle bone before occurrence of spontaneous fractures. *Bone* 29:271-278, 2001

17. Nagelberg A: Musculoskeletal conditions in the U.S. *The American Academy of Orthopaedic Surgeons Bulletin*, American Academy of Orthopaedic Surgeons, 47:5, 10, 1999

18. Park JB: *Biomaterials Science and Engineering*, pp 389-394. New York, Plenum Press, 1984

19. Rice JC, Cowin SC, Bowman JA: On the dependence of the elasticity and strength of cancellous bone on apparent density. *J Biomech* 21:155-168, 1988

20. R∅hl L, Larsen E, Linde F, Odgaard A, J∅rgensen: Tensile and compressive propertied of cancellous bone. *J Biomech* 24:1143-1149, 1991

21. Schaldach M, Hohmann D, Thull R, Hein F, editors: *Advances in Artificial Hip and Knee Joint Technology*, pp 90-104, 182-184. Berlin, Springer-Verlag, 1976

22. Silva MJ, Gibson LJ: Modeling the mechanical behavior of vertebral trabecular bone: effect of age-related changes in microstructure. *Bone* 21:191-199, 1997

23. Tortora GJ: *Principles of Human Anatomy*, 7th Ed, pp 166-171, 196-201. New York, HarperCollins College, 1995

24. Watts NB: Bone quality: getting closer to a definition. *J Bone Miner Res* 17:1148-1150, 2002

25. Wolf S, Augat P, Wan S, Claes L: Experimental investigations for the prediction of the mechanical stability of regions of cancellous bone. *J Biomech* 31:37, 1998

26. Yeh OC, Keaveny TM: Biomechanical effects of intraspecimen variations in trabecular architecture: a three-dimensional finite element study *Bone* 25:223-228, 1999

27. Yeni YN, Fyhrie DP: Finite element calculated uniaxial apparent stiffness is a consistent predictor of uniaxial apparent strength in human vertebral cancellous bone tested with different boundary conditions. *J Biomech* 34:1649-1654, 2001

**VITA**

Danu Prommin was born in Bangkok, Thailand on July 21, 1973. He attended King Mongkut's Institute of Technology in Thonburi, Thailand where he received his Bachelor of Engineering in industrial engineering in March of 1994. Danu Prommin enrolled in the Biomedical Engineering Program at Texas A&M University, College Station, TX in the fall of 1998, receiving his Master of Science in biomedical engineering in August 2000, and his Doctor of Philosophy in biomedical engineering in August 2004.

Danu Prommin's permanent address is

14 Chaleom-Phrakiat Rama 9 Soi 14

Sukumwit 103, Nongbond, Prawait

Bangkok, 10250

Thailand